PERMEABILITY THEORY FOR POLYDISPERSED COLLOIDAL CAKES AND ANALYSIS OF MEMBRANE BIOREACTOR (MBR) MODELS

A THESIS SUBMITTED TO THE GRADUATE DIVISION OF THE UNIVERSITY OF HAWAI'I IN PARTIAL FULFILLMENT OF THE REQUIREMENTS FOR THE DEGREE OF

MASTER OF SCIENCE

IN

CIVIL ENGINEERING

AUGUST 2006

By
Aileen Ng

Thesis Committee:

Albert S. Kim, Chairperson
Roger W. Babcock
Michelle H. Teng

We certify that we have read this thesis and that, in our opinion, it is satisfactory in scope and quality as a thesis for the degree of Master of Science in Civil Engineering.

THESIS COMMITTEE

Albert S. Kim

Chairperson

Roger Babcock Jr

Michael Eng Tong

ACKNOWLEDGMENTS

I would like to express my deep gratitude to my advisor, Dr. Albert S. Kim, for his patience, understanding, and wisdom as he guided me through the process of completing this thesis. Special thanks to the other members of my committee, Dr. Michelle H. Teng and Dr. Roger W. Babcock, for taking the time to review my thesis and for offering their comments and suggestions. I would also like to acknowledge Ms. Carrie Matsuzaki for proofreading my thesis.

Thanks to the members of the Colloid Research Group for their encouragement and fellowship. Warm thanks go to Kyle, Rose, and other dear friends for their love and prayers that have carried me through the year. Finally, I am forever grateful to my family for their constant love and care. Their support has enabled me to complete this work.

ABSTRACT

Models can serve as valuable tools for understanding, designing, and optimizing membrane filtration systems, which are commonly used for the treatment of water and wastewater. Two areas in the modeling of membrane technology that are lacking in development include the characterization of polydispersed colloidal fouling and the modeling of membrane bioreactor (MBR) systems. In this study, new analytical expressions are introduced for calculating the permeability of polydispersed cakes composed of spherical particles with log-normal and normal particle size distributions (PSD). Comparison of the permeabilities show that normal PSDs consistently exhibit lower permeability than log-normal cases due to the larger number of smaller particles in normal PSDs. Additionally, a review and assessment of current modeling efforts on MBRs for municipal wastewater treatment were conducted. The review confirmed that MBR model development is still in its early stages, and much research is needed in the area.

TABLE OF CONTENTS

LIST OF TABLES

TABLE PAGE

LIST OF FIGURES

FIGURE PAGE

CHAPTER 1. INTRODUCTION

Membranes are semipermeable, thin-layered materials that can selectively separate suspended and dissolved solids from water on the basis of size and molecular weights. Since the development of the synthetic asymmetric membranes in the 1960s, there has been steadily growing interest in the application of pressure-driven membrane processes for water and wastewater treatment. Factors contributing to this substantial growth include increasing stringency of water quality regulations and growing water demands that make it necessary to exploit lower quality water resources. Membrane processes are capable of producing higher quality effluent than conventional treatment processes, and they enable the use of water resources, such as seawater and wastewater, which were previously inaccessible due to technological and economical limitations. The move toward privatization in the water industry and the opening up of world treatment markets have also led to the development of more innovative treatment technologies involving membrane filtration (Mallevialle et al. 1996). While these factors create a market for membrane systems, further expansion of the technology relies on the ability to overcome technical and economic problems associated with industrial-scale applications of membrane filtration. The ability to model membrane systems is essential as models can aid in the advancement of the technology by serving as tools for understanding, designing, and optimizing systems. Two less-developed areas in membrane process

modeling are the characterization of polydispersed colloidal fouling and membrane bioreactor systems, which are examined in this study.

Permeate flux and influencing factors are important considerations in determining the performance and cost of membrane systems. Membrane fouling is a major limitation of the technology as it leads to permeate flux decline and necessitates frequent cleaning, later followed by membrane replacement. Fouling lessens the duration of permeate production and increases the operating and maintenance costs of the system. One of the largely studied membrane fouling mechanisms in microfiltration (MF) and ultrafiltration (UF) processes is cake formation stemming from particle deposition on the membrane surface. Cakes generate additional hydraulic resistance, which results in reduced permeate flux. A plethora of experimental and theoretical studies have been performed to investigate this fouling phenomenon. However, for simplification, many approaches consider only ideal and well-controlled cases. A frequently used ideal situation assumes monodispersed particles in the feed suspension, though this is rarely encountered under actual conditions. Very few studies have been conducted to examine the effects of particle polydispersity on water permeation of MF and UF processes, and fundamental expressions of the polydispersed cake permeability are still lacking in the literature. In this study, expressions are derived for the permeability of media composed of polydispersed spherical particles by considering two typical ideal particle size distributions (PSDs).

The membrane bioreactor (MBR) is a single processsystem that combines membrane filtration with biological. MBR systems typically use MF and UF membranes.

MBRs have been recognized as a valuable technology for wastewater treatment because of the advantages that they provide over conventional biological treatment processes. In the treatment of municipal wastewater, MBRs have demonstrated the ability to produce high-quality effluent, with the reported capability of removing 95, 98, and 99 percent (or greater) of chemical oxygen demand (COD), biochemical oxygen demand (BOD) and suspended solids (SS), respectively (Manem and Sanderson 1996). MBRs provide greater independent control over the solids retention time (SRT) and hydraulic retention time (HRT) as membrane filtration (rather than gravitational settling) separates the biomass from the effluent. This allows for operation at a longer SRT and higher loading rates, which results in less sludge production and shortens the necessary HRT (Tchobanoglous et al. 2004) . Also, MBR systems require less space as the use of membranes eliminates the need for large clarifying basins to settle out the biomass. Complex yet practical models can greatly assist in capitalizing on the benefits of MBR technology. However, membrane bioreactors are a relatively young technology and the extent of MBR model development is still at a rudimentary stage.

This study examines two areas in membrane process modeling that are in need of more research efforts. Colloidal fouling is considered in chapter 2, where new analytical expressions are introduced for calculating the permeabilities of polydispersed cakes composed of spherical particles with log-normal and normal particle size distributions. Chapter 3 presents a review and assessment of current MBR modeling efforts with the aim to facilitate MBR model development. Parameters are identified that require accurate modeling, and suggestions are made for future work in model development for MBRs.

CHAPTER 2. PERMEABILITY THEORY FOR POLYDISPERSED CAKES

2.1 Introduction to Permeability and Polydispersity

Membrane fouling leads to permeate flux decline and is a major problem encountered in membrane filtration technologies. A common fouling mechanism in microfiltration (MF) and ultrafiltration (UF) processes is cake formation from particle deposition on the membrane surface, which causes additional hydraulic resistance to water permeation. Many studies have applied different approaches, both experimental and theoretical, to explain and quantify the fouling phenomenon. However, these studies commonly assume monodispersed particles in the feed suspension and do not account for distribution in size of particles found in natural waters.

The quantification of cake resistance is important because it relates permeate flux to transmembrane pressure. Essential in the operation of water and wastewater treatment plants is the ability to quantify the ratio of production to operating cost (i.e., the permeate flux to the energy required to achieve that flux). Numerous models have been introduced to compute the specific cake resistance (i.e., inverse hydraulic permeability) of porous media composed of equal-sized spherical particles, which can then be multiplied by the thickness of the medium to yield the cake resistance. Three most commonly used models to estimate the hydraulic resistance of the porous media are the Carmen-Kozeny model (Carman 1937), the Brinkman model (Brinkman 1947; Brinkman 1947), and Happel's cell model (Happel 1958). Although these models can generate reasonable estimates of

the hydraulic resistance of cake layers, they are based on porous media composed of uniformly-sized particles.

Very few studies consider the effects of particle polydisperisty on water permeation in MF and UF processes. The several studies found in literature that examine this effect apply vastly different approaches. Gmachowski presented a method to quantify the permeability of a polydispersed cake (Gmachowski 1998). He demonstrated that a porous media of polydispersed particles is hydraulically comparable to a packed bed of uniformly-sized particles with an equivalent effective radius. The polydispersed porous media was then likened to a dense system of permeable aggregates, and based on this artificial transformation, an expression for the effective particle radius was derived in terms of the aggregate fractal dimension. Lu and Tsai applied micro-scale computation to simulate the microstructures formed by the deposition of two-dimensional circular particles (disks) with uniform, normal, and log-normal size distributions (Lu and Tsai 2000). The transition parameter (which determines the weight of the competing deterministic and non-deterministic forces), incident angle of release, and number of post-contact rollings were varied to control the deposition conditions. The resulting microstructures were studied in terms of their porosity, mean height, and other characteristics. Observations from this 2D case were used to imply 3D phenomenon. Chellam employed artificial neural networks to predict an instantaneous specific flux (the ratio of the instantaneous permeate flux and transmembrane pressure) from a set of inputs expected to influence membrane fouling (Chellam 2005). The neural networks were trained with three sets of partial data from experiments where the degrees of

polydispersivity of the feed suspensions were varied. The accuracy of the neural network predictions were evaluated against the complete data sets.

Fundamental expressions of the polydispersed cake permeability are still lacking in the literature. To the best of our knowledge, no published studies present equations to compute the permeability of polydispersed porous media, aside from that by Gmachowski. In this study, two analytical expressions are derived for calculating the permeability of porous media composed of spherical particles with log-normal and normal PSDs. A similar approach to that of Gmachowski's is taken, but an entirely different method is used to derive expressions for the effective particle radii.

2.2 Derivation of the Permeability Expressions

A single particle in a uniform flow field, as illustrated in Fig. 1(a), experiences a hydrodynamic drag force that can be rigorously represented by Stokes law (Lamb 1932; Bird et al. 1960):

$$F_{Stokes} = 6\pi\mu a U \tag{1}$$

Here, μ is the absolute fluid viscosity, a is the particle radius, and U is the uniform approaching fluid velocity. To maintain the same approaching fluid velocity through a swarm of polydispersed particles, shown in Fig. 1(b), a higher pressure must be applied. The drag force experienced by a single particle in a swarm of other particles is, therefore, greater than that experienced by an isolated particle. A hydraulic correction factor, $\Omega(>1)$, can be used to correct the drag force for the increased pressure (Carman 1937; Brinkman 1947; Happel 1958; Happel and Brenner 1965; Howells 1974; Hinch 1977;

Kim and Russel 1985). The total drag force exerted on a cake layer composed of N particles of varying sizes can then be expressed as (Russel et al. 1989; Gmachowski 1998):

$$F = \sum_{i=1}^{N} 6\pi\mu a_i \Omega_i U \tag{2}$$

where $i(=1,2,...,N)$ is the particle index. The total volume V of the cake layer, including void spaces, is found by dividing the sum of the volume of the individual particles by the cake volume fraction, ϕ:

$$V = \frac{\sum_{i=1}^{N} \frac{4\pi}{3} a_i^3}{\phi} \tag{3}$$

Dividing the total drag force exerted on the cake layer by the total cake layer volume gives the hydrodynamic force density, which can be equated to the pressure gradient across the cake layer:

$$\frac{F}{V} = \frac{\sum_{i=1}^{N} 6\pi\mu a_i \Omega_i U}{\frac{\sum_{i=1}^{N} \frac{4\pi}{3} a_i^3}{\phi}} = \frac{\mu U}{\kappa} \tag{4}$$

Here, κ is the cake permeability (i.e., the inverse of the specific cake resistance, r_c). Since the fluid is incompressible, the fluid velocity U is the approaching velocity at the top of the cake layer, and therefore, the permeate velocity. Expressing Eq. (4) in terms of the permeability yields

$$\kappa = \frac{2\left(\frac{1}{N}\sum_{i=1}^{N} a_i^3\right)}{9\phi\left(\frac{1}{N}\sum_{i=1}^{N} a_i\Omega_i\right)} = \frac{2\langle a^3\rangle}{9\phi\langle a\Omega\rangle} \tag{5}$$

If it is assumed that the hydrodynamic forces acting on all particles are uniformly corrected, i.e.,

$$\langle a\Omega\rangle \simeq \langle a\rangle\langle\Omega\rangle \simeq \langle a\rangle\Omega(\phi) \tag{6}$$

Eq. (5) can be rewritten as

$$\kappa = \frac{2}{9\phi\Omega} a_{\text{eff}}^2 \tag{7}$$

where a_{eff} is defined as

$$a_{\text{eff}} = \sqrt{\frac{\langle a^3\rangle}{\langle a\rangle}} \tag{8}$$

and is termed the effective radius. Thus, a sphere-packed medium composed of particles of different sizes is hydraulically equivalent to a monodispersed medium with a particle radius equal to the effective radius of the particles in the polydispersed medium.

Two common model distributions of particle sizes are the log-normal and normal (Gaussian) distributions. In the following sections, the effective radius and permeability of media composed of particles with log-normally distributed and normally distributed particle sizes are derived.

2.2.1 Log-Normal Distribution

The log-normal distribution of particle radii a is

$$L(a) = \frac{1}{\sqrt{2\pi}\beta a} \exp\left(-\frac{\left[\ln(a/a_0)\right]^2}{2\beta^2} \right) \tag{9}$$

where a_0 and β are the geometric mean and geometric standard deviation of the PSD, respectively, and can be determined by experiment. The raw moment, $\langle a^n \rangle$, of the probability density function is defined as

$$\langle a^n \rangle \equiv \int_{a=0}^{\infty} a^n L(a) \mathrm{d}a \tag{10}$$

Solving the integral in Eq. (10), one can obtain

$$\langle a^n \rangle = a_0^n \exp\left(\frac{n^2 \beta^2}{2} \right) \tag{11}$$

and the following expressions for $\langle a \rangle$, $\langle a^2 \rangle$, and $\langle a^3 \rangle$:

$$\langle a \rangle = a_0 e^{\frac{1}{2}\beta^2} \tag{12}$$

$$\langle a^2 \rangle = a_0^2 e^{2\beta^2} = \langle a \rangle^2 e^{\beta^2} \tag{13}$$

$$\langle a^3 \rangle = a_0^3 e^{9\beta^2/2} = \langle a \rangle^3 e^{3\beta^2} \tag{14}$$

From Eqs. (8) and (14), the effective radius can then be expressed as

$$a_{\mathrm{eff}} = \sqrt{\frac{\langle a^3 \rangle}{\langle a \rangle}} = \langle a \rangle e^{\frac{3}{2}\beta^2} \tag{15}$$

and the permeability of cake composed of particles with log-normally distributed particle radii is given by

$$\kappa_L = \frac{2}{9\phi\Omega} \langle a \rangle^2 e^{3\beta^2} \tag{16}$$

For a distribution of particle radii, the standard deviation σ is

$$\sigma = \sqrt{\langle a^2 \rangle - \langle a \rangle^2} \tag{17}$$

Substituting Eqs. (12) and (13) into Eq. (17), the standard deviation of particle radii can be expressed as

$$\sigma = \sqrt{\langle a \rangle^2 e^{\beta^2} - \langle a \rangle^2} = \sqrt{\langle a \rangle^2 \left(e^{\beta^2} - 1\right)} = \langle a \rangle \sqrt{\left(e^{\beta^2} - 1\right)} \tag{18}$$

The values of a_0 and β can be computed from Eqs. (12) and (18) using experimentally determined values of mean $\langle a \rangle$ and standard deviation σ of particle radii. Then, the permeability of cakes with log-normally distributed particle sizes can be calculated from Eq. (16), knowing the cake volume fraction (which can be determined from experiment) and hydraulic correction factor (which can be computed knowing the cake volume fraction).

2.2.2 Normal Distribution

A normal distribution of particle radii is described as

$$N(a) = \frac{1}{\sqrt{2\pi}\sigma} \exp\left(-\frac{\left(a - \langle a \rangle\right)^2}{2\sigma^2} \right) \tag{19}$$

where $\langle a \rangle$ and σ are the mean and standard deviation, respectively. Again, the mathematical definition for the raw moment in Eq. (10) is applied here:

$$\langle a^n \rangle \equiv \int_0^\infty a^n N(a) \mathrm{d}a \tag{20}$$

and following approximation is made:

$$\langle a^n \rangle \approx \int_{-\infty}^{\infty} a^n N(a) \mathrm{d}a \tag{21}$$

This approximation is valid when $\langle a \rangle$ is greater than 2σ since the range of the normal distribution is roughly 4σ (Mendenhall et al. 2003). Solving Eq. (21) for $n = 3$ yields

$$\langle a^3 \rangle = \langle a \rangle \left(\langle a \rangle^2 + 3\sigma^2 \right) \tag{22}$$

The effective radius of normal distribution of particle radii is then

$$a_{\mathrm{eff}} = \sqrt{\langle a \rangle^2 + 3\sigma^2} \tag{23}$$

and the hydraulic permeability is

$$\kappa_N = \frac{2\langle a \rangle^2}{9\phi\Omega} \left(1 + \frac{3}{4} \left(\frac{2\sigma}{\langle a \rangle} \right)^2 \right) \tag{24}$$

As with the log-normal case, the cake layer permeability (and specific cake resistance) can be computed from the mean and standard deviation of the particle sizes, the average cake volume fraction, and the hydraulic correction factor.

2.3 Comparison of the Permeabilities for Normal and Log-Normal PSDs

To compare the permeability of cakes composed of particles with a normal versus log-normal size distribution, an expression for the ratio of the permeabilities with the same mean particle size and standard deviation was derived. Eqs. (12) and (18) were substituted into Eq. (19) and then divided by Eq. (16) to obtain the following:

$$\frac{\kappa_N}{\kappa_L} = e^{-3\beta^2} \left(3e^{\beta^2} - 2 \right) \tag{25}$$

The plot of this ratio as a function of β, shown in Fig. 2, reveals that the normal distribution exhibits a lower permeability than the log-normal distribution for all $\beta > 0$. This indicates that cake layer composed of particles with a normal PSD will have a higher specific resistance than that composed of particles with a log-normal PSD with the same mean and standard deviation.

Insight into the source of the lower permeability for a normal distribution can be gained by comparing the plots of the mean-scaled distributions, defined as:

$$\langle a \rangle L(r) = \frac{1}{\sqrt{2\pi}\beta r} \exp\left(-\frac{1}{2\beta^2} \left[\frac{\beta^2}{2} + \ln(r) \right]^2 \right) \tag{26}$$

$$\langle a \rangle N(r) = \frac{1}{\sqrt{2\pi\left(e^{\beta^2} - 1\right)}} \exp\left(-\frac{(r-1)^2}{2\left(e^{\beta^2} - 1\right)} \right) \tag{27}$$

where $r = a/\langle a \rangle$. Fig. 3 shows the scaled distributions plotted for $\beta = 0.3$. From Fig. 3, it is observed that the normal distribution has a larger number of smaller particles than the log-normal distribution, as indicated by the longer tail near $r = 0$. These small particles contribute to a larger specific cake resistance since they can fill in the voids formed by larger particles. It is assumed in this study that each particle occupies approximately an equal spatial fraction of volume, which is the cake volume fraction.

The observation of lower permeability for the normal PSD can be viewed in another manner. Recall from Eq. (7) that a sphere-packed medium of polydispersed particles can be hydraulically represented as a medium of homogenously and

isotropically distributed, monodispersed particles with a radius equal to an effective radius as defined in Eq. (8). The permeability of the polydispersed medium is proportional to the square of the effective radius. Therefore, the distribution with the smaller effective radius will display the lower permeability. A comparison of the dimensionless effective radii, $a_{\text{eff}}/\langle a \rangle$, for the log-normal and normal distributions (in Eqs. (15) and (23), respectively) with the same mean and standard deviation is shown in Fig. 4. For $\beta = 0.8$, the effective radius of the log-normal distribution is 1.36 times greater than that of the normal distribution. This means that if a cake layer composed of spherical particles with normally distributed particle sizes is mapped to a monodispersed cake layer with particle radius a', a cake layer with log-normally distributed particles sizes can be equivalently treated as a monodispersed cake layer composed of particles with radius $1.36a'$. Generally, for $\beta > 0$, the effective radius of the normal distribution is smaller than that of the log-normal distribution. This is due to the larger number of smaller particles that contribute to a smaller effective radius. Thus, the normal distribution exhibits a lower permeability.

2.4 Application of the Permeability Expressions

For MF and UF membranes, in which size exclusion is the primary mechanism for separation, cake resistance (R_c) can significantly influence the permeate flux (U). This is demonstrated by Darcy's law:

$$U = \frac{\Delta P}{\mu\left(R_m + R_c\right)} \tag{28}$$

where μ is the absolute solvent viscosity, and R_m is the intrinsic membrane resistance. When the cake resistance is high relative to the membrane resistance, the decrease in permeate flux can be remarkable for an applied pressure. The permeability expressions can be used to calculate the cake resistance in the following manner. The specific cake resistance (r_c) can be computed by simply taking the inverse of the permeability:

$$r_c = \frac{1}{\kappa} \tag{29}$$

and the cake resistance can be found by multiplying the specific cake resistance by the cake layer thickness (δ_c):

$$R_c = r_c \delta_c \tag{30}$$

Recall the assumption in this study of equal spatial fraction of volume occupied by each particle. This assumption is motivated by the work of Soppe (Soppe 1990), which demonstrates that the vertical density profile of sediments is uniform and homogenous regardless of its polydispersity, i.e., standard deviation of particle size in a Gaussian distribution. However, it is also noted that this assumption may not be fully valid under certain conditions. Indirect experimental studies have shown that the particle's size and mass density can dictate the stratification of a cake layer (Soppe 1990; Knight et al. 1993; Breu et al. 2003). This phenomenon is complicated when several different kinds of particulate material with their own polydispersity exist in the feed solution. Where shear-induced diffusion plays a crucial role in the back-diffusion of particles from the membrane surface to the bulk phase, the cake layer will become noticeably stratified with the bottom section consisting mainly of small particles (Davis

and Birdsell 1987; Davis and Leighton 1987; Leighton and Acrivos 1987; Romero and Davis 1988; Davis and Sherwood 1990; Sethi and Wiesner 1997; Chellman and Wiesner 1998; Mondor and Moresoli 2000). The major resistance will stem mainly from the smaller particles deposited on the membrane surface, and larger particles will not contribute significantly to the cake resistance. However, if entropic (Brownian) influences are the dominant hydrodynamic effect, the cake structure will have a random, well-mixed, and (macroscopically) uniform distribution of polydispersed particles throughout the entire layer, and larger particles will play a beneficial role in permeate production. The approach presented in this study is applicable in this latter case.

CHAPTER 3. ANALYSIS OF MEMBRANE BIOREACTOR MODELS

3.1 Review and Assessment of Modeling Studies on Membrane Bioreactors

A review and assessment of published works is presented in this chapter on the modeling of the MBR process for the treatment of municipal wastewaters. The complete model equations can be found in Appendix A. The models are considered in three categories. The first three models, i.e., the activated sludge model family, the soluble microbial products model, and the ASM1-SMP hybrid model, describe the biomass kinetics in biological treatment. The next three are membrane fouling models, which include the empirical hydrodynamic model, fractal permeation model, and sectional resistance model. The last two models are integrated models, which combine a biomass kinetics model and a membrane fouling model to describe the complete MBR system.

3.1.1 The Activated Sludge Model (ASM) Family

In 1983, the International Association on Water Pollution Research and Control (IAWPRC), later known as the International Association on Water Quality (IAWQ) and now as the International Water Association (IWA), formed a task group to develop a practical model for the design and operation of the biological wastewater treatment process. The product of the group's efforts is the activated sludge model no. 1 (Henze et al. 1987), introduced in 1987. Other models introduced by the association in later years expanded and improved upon the first model. These include the activated sludge model

no. 2 (Henze et al. 1995), which incorporates phosphorus removal from wastewaters; the activated sludge model no. 2d (Henze et al. 1999), which takes into account the ability of phosphorus accumulating organisms to use cell internal substrates for denitrification; and the activated sludge model no. 3 (Gujer et al. 1999), which does not include modeling phosphorus removal but addresses problems found in the first model.

Although the activated sludge models were developed to describe the conventional activated sludge process, it has been suggested in literature that the models can be used to simulate biomass kinetics in an MBR system (Lu et al. 2001; Lee et al. 2002; Wintgens et al. 2003). The MBR process is the activated sludge process with the secondary clarification step replaced by membrane filtration. Therefore, it is reasonable to use the ASMs to characterize the biomass dynamics in an MBR system. Presented here is a brief overview of the four ASMs. The IWA Task Group publication (Henze et al. 2000) should be referred to for more details on the models' components, processes, calibration methods, applications, and limitations.

3.1.1.1. Activated Sludge Model No.1 (ASM1)

The activated sludge model no. 1 was developed to model biological treatment for organic carbon removal, nitrification, and denitrification. The model can be used to predict oxygen demand and sludge production in an activated sludge system. There are two main concepts that have been incorporated into the model. The first concept is that biodegradable COD in wastewater is composed of readily biodegradable COD (RBCOD) and slowly biodegradable COD (SBCOD). The RBCOD can immediately be used by organisms for synthesis, whereas the SBCOD must be broken down before it can pass

through the organism's cell wall to be metabolized. Total COD in the model is comprised of biodegradable COD (SBCOD and RBCOD), non-biodegradable COD (i.e., inert material), and the active biomass. The second concept is the death-regeneration concept. When the biomass decays, a portion of the decayed cell material is non-biodegradable and remains inert. The rest of the decayed material is slowly biodegradable and can be broken down to be used by active organisms for growth.

Shown in Fig. 5 are the main processes captured in the model, i.e. the hydrolysis of slowly biodegradable material and the growth and decay of the organisms in the biomass. There are two groups of organisms considered in the model: autotrophs ($X_{B,A}$) and heterotrophs ($X_{B,H}$). The autotrophs perform the nitrifying activities. Their growth occurs through the oxidation of ammonia (S_{NH}) to nitrate (S_{NO}), which transpires only under aerobic conditions. This process is modeled by saturation-type (Monod) kinetics. Heterotrophs perform the carbon removal and denitrification. They consume soluble substrate (S_S) and ammonia for growth under both aerobic and anoxic conditions. Under aerobic conditions, oxygen is utilized in the growth process. In anoxic conditions, where oxygen is absent, nitrate is used as the electron acceptor and is reduced to dinitrogen. The heterotrophic growth process is likewise modeled by saturation-type kinetics. The decay processes for both types of organisms are as described by the death-regeneration concept, although only heterotrophs can reuse the biodegradable decay material for growth. The decay process is assumed to follow first order kinetics, though the autotrophic decay rate is slower.

The basic structure of ASM1 is a mass balance to describe the accumulation rate of a particular component within the system:

$$Accumulation = Input - Output + Reaction$$

The model supplies expressions of reaction rates for the various model components, so that they can be applied to many different process configurations. A matrix format is used to allow for easy identification of the rate processes that affect the fate of each component. A section of the ASM1 matrix is shown in Table 1. The reaction rate r of a

Table 1. A section of the matrix of process kinetics and stoichiometry from ASM1

Component i		6	7	8	Process Rate, ρ_j
j	Process	$X_{B,A}$	X_P	S_O	$[ML^{-3}T^{-1}]$
1	Aerobic growth of heterotrophs			$-\frac{1-Y_H}{Y_H}$	$\hat{\mu}_H\left(\frac{S_S}{K_S+S_S}\right)\left(\frac{S_O}{K_{O,H}+S_O}\right)X_{B,H}$
3	Aerobic growth of autotrophs	1		$-\frac{4.57-Y_A}{Y_A}$	$\hat{\mu}_A\left(\frac{S_{NH}}{K_{NH}+S_{NH}}\right)\left(\frac{S_O}{K_{O,A}+S_O}\right)X_{B,A}$
4	Decay of heterotrophs		f_P		$b_H X_{B,H}$
5	Decay of autotrophs	-1	f_P		$b_A X_{B,A}$

component i can be read from the matrix by traversing down column i and summing the products of the coefficient, ν_{ij}, and the corresponding process rate ρ_j:

$$r_i = \sum_j \nu_{ij}\rho_j \tag{31}$$

If there is no coefficient listed on the table, the coefficient is zero. To demonstrate, the reaction rate for autotrophic biomass, $X_{B,A}$, is

$$r_{X_{B,A}} = 1 \cdot \hat{\mu}_A \left(\frac{S_{NH}}{K_{NH} + S_{NH}} \right) \left(\frac{S_O}{K_{O,A} + S_O} \right) X_{B,A} + (-1) \cdot b_A X_{B,A}$$

and the reaction rate for particulates arising from biomass decay, X_P, is

$$r_{X_P} = f_p \cdot b_H X_{B,H} + f_p \cdot b_A X_{B,A}$$

In the model, $\mu_?$ denotes a maximum growth rate, $K_?$ is a saturation coefficient, and $b_?$ is a rate constant. Thirteen components are incorporated in the model, and a mass balance equation can be derived for each of these components from the eight rate processes listed in Table 2. The inert material, X_I and S_I, are incorporated in the model despite having a zero reaction rate because X_I becomes enmeshed in the activated sludge and removed from the system through sludge waste, and S_I leaves the system at the same concentration that it enters. All organic material and biomass components are expressed in terms of COD because it can be used to link organic substrates, biomass, and consumed oxygen by electron equivalents. Likewise, oxygen is expressed as negative oxygen demand.

A number of simple assumptions are made in this model, which impose limitations on its application. One assumption is that the system operates at constant temperature. Temperature fluctuations can be adjusted for by applying the Arrhenius equation to express thermal sensitivity of model parameters in the rate expressions. The model also assumes system operation at constant pH near neutral. Although it is known that pH may influence some model parameters, few expressions exist to capture this influence. Alkalinity has been included in the model to allow detection of problems with pH control. The model parameters in the rate expression are assumed to be constant. Consequently, the model does not handle changes in wastewater characteristics. The

Table 2. Components and rate processes in ASM1, ASM2, and ASM3

	Components	Processes
ASM1	Soluble inert organic matter (S_I) Readily biodegradable substrate (S_S) Particulate (suspended) inert organic matter (X_I) Slowly biodegradable substrate (X_S) Active heterotrophic biomass ($X_{B,H}$) Active autotrophic biomass ($X_{B,A}$) Particulates arising from biomass decay (X_P) Oxygen (negative COD) (S_O) Nitrate and nitrite nitrogen (S_{NO}) Ammonia and ammonium nitrogen (S_{NH}) Soluble biodegradable organic nitrogen (S_{ND}) Particulate biodegradable organic nitrogen (X_{ND}) Alkalinity (S_{ALK})	Aerobic growth of $X_{B,H}$ Anoxic growth of $X_{B,H}$ Aerobic growth of $X_{B,A}$ Decay of $X_{B,H}$ Decay of $X_{B,A}$ Ammonification of S_{ND} Hydrolysis of entrapped organics Hydrolysis of entrapped organic nitrogen
ASM2	Dissolved oxygen (S_{O2}) Fermentable (readily biodegradable substrate (S_F) Fermentation products (S_A) Ammonium and ammonia nitrogen (S_{NH4}) Nitrate and nitrite nitrogen (S_{NO3}) Inorganic soluble phosphorus (S_{PO4}) Inert soluble organic material (S_I) Alkalinity (S_{ALK}) Dinitrogen (S_{N2}) Inert particulate organics (X_I) Slowly biodegradable substrates (X_S) Heterotrophic organisms (X_H) Phosphate accumulating organisms (X_{PAO}) Poly-phosphates (X_{PP}) Cell internal storage products of PAO (X_{PHA}) Nitrifing organisms (X_{AUT}) Total suspended solids (X_{TSS}) Metal hydroxides (X_{MeOH}) Metal-phosphate (X_{MeP})	Aerbobic hydrolysis Anoxic hydrolysis Anaerobic hydrolysis Aerobic growth of X_H on S_F Aerobic growth of X_H on S_A Anoxic growth of X_H on S_F Anoxic growth of X_H on S_A Fermentation Lysis of X_H Storage of X_{PHA} Storage of X_{PP} Aerobic growth of X_{PAO} on X_{PHA} Lysis of X_{PAO} Lysis of X_{PP} Lysis of X_{PHA} Aerobic growth of X_{AUT} Lysis of X_{AUT} Precipitation of S_{PO4} Redissolution of S_{PO4}
ASM3	Dissolved oxygen (negative COD) (S_O) Inert soluble organic matter (S_I) Readily biodegradable organic substrate (S_S) Ammonium plus ammonia nitrogen (S_{NH4}) Dinitrogen (S_{N2}) Nitrate and nitrite nitrogen (S_{NOX}) Alkalinity (S_{ALK}) Inert particulate (suspended) organic matter (X_I) Slowly biodegradable substrate (X_S) Active heterotrophic organisms (X_H) Cell internal storage product of heterotrophic organisms (X_{STO}) Nitrifying organisms (X_A) Suspended solids (X_{SS})	Hydrolysis Aerobic storage of S_S Anoxic storage of S_S Aerobic growth of X_H Anoxic growth of X_H Aerobic endogenous respiration of X_H Anoxic endogenous respiration of X_H Aerobic endogenous respiration of X_{STO} Aerobic endogenous respiration of X_{STO} Aerobic growth of X_A Aerobic endogenous respiration of X_A Anoxic endogenous respiration of X_A

effects of low nutrient concentrations (e.g., phosphorous, nitrogen, and other inorganic nutrients) on the removal of organic substrate and cell growth are not considered specifically. It is presumed that sufficient quantities of nutrients are present to allow for balanced growth of organisms. Although the biomass may change in species diversity over time, the kinetic parameters remain fixed in the model, as it would be too complicated to capture such effect on the kinetic parameters. Other assumptions made in the model include constant value for nitrification-related parameters, which are presumed to incorporate inhibitory effects of waste constituents, instantaneous entrapment of particular organics by the biomass, coupled and simultaneous occurrence of the hydrolysis of organic matter and organic nitrogen at equal rates, and indifference of the electron acceptor type on the biomass decay.

3.1.1.2. Activated Sludge Model No.2 (ASM2)

The activated sludge model no. 2, presented in 1995, expands upon ASM1 to primarily include biological phosphorous removal. In addition to heterotrophs and autotrophs, a new group of organisms called phosphorus accumulating organisms (PAO) is incorporated in the biomass to encompass the different types of microorganisms capable of accumulating phosphorous and storing them in the form of cell internal polyphosphates (X_{PP}). The PAO are assumed to be incapable of denitrifying activity and can only grow on stored cell internal organic material, X_{PHA}. Fig. 6 shows the storage and growth processes of PAO incorporated in ASM2. PAO will store external fermentation products (S_A) in the form of internal cell storage material (X_{PHA}) primarily under anaerobic conditions. The energy for this process comes from the hydrolysis of X_{PP},

which leads to the release of soluble phosphates (S_{PO4}). The kinetic expression for the storage of X_{PHA} does not include inhibition terms for dissolved oxygen and nitrate plus nitrite nitrogen because this process has been reported to occur under aerobic and anoxic conditions. Phosphates are also stored in the form of X_{PP}, with the energy supplied from the respiration of X_{PHA}. The X_{PP} is regenerated because PAO require S_A stored in the form of X_{PHA} for growth, and the storage of S_A requires the release of X_{PP}. According to the model, the growth of PAO transpires only under aerobic conditions. The process occurs at the expense of X_{PHA} and involves the consumption of S_{PO4} and lysis of X_{PP}. Separate process rates are provided in the model for the lyses of PAOs and the two storage products to capture all losses of biomass that occur due to respiration and maintenance or death.

In ASM2, the growth of heterotrophic organisms occur under both aerobic and anoxic conditions from the consumption of fermentable substrates (S_F) and fermentation products (S_A), yielding four separate growth processes. The growth rates μ_m and yield coefficients Y_H are assumed to be identical for both aerobic and anoxic processes. Under aerobic conditions, heterotrophic growth processes consume oxygen (S_{O2}), nutrients (S_{NH4} and S_{PO4}), and possibly alkalinity (S_{ALK}) to produce suspended solids (X_{TSS}). The anoxic growth processes utilize nitrate (S_{NO3}) instead of oxygen, and the nitrate is reduced to dinitrogen (S_{N2}). Denitrification, which releases alkalinity, is assumed to be inhibited by the presence of oxygen (S_{O2}), and the maximum growth rate is reduced relative to that under aerobic conditions. The slower growth rate accounts for the fact that not all heterotrophs are capable of performing denitrification reactions. In anaerobic conditions,

where both oxygen and nitrate are not available, fermentation is assumed to occur. In this process S_F is directly transformed by heterotrophs to S_A, and alkalinity is required due to the electric negativity of S_A. Processes involving autotrophic organisms are the same as in ASM1, except rate limitations imposed by phosphate concentrations are incorporated into the rate expression for autotrophic growth.

Two additional rate processes (precipitation and redissolution of phosphates) and two components (metal-hydroxides and metal phosphates) were included in ASM2 to capture the precipitation and redissolution of phosphates. Metals are naturally present in wastewater and can precipitate with released soluble ortho-phosphates if both constituents exist in high enough concentrations. It is also common practice to add iron or alum salts to aid in phosphorous removal through chemical precipitation. The ASM2 models these reactions.

Table 2 lists the 19 components and 19 rate processes in the ASM2 model. The same model limitations of ASM1 apply to ASM2. Further assumptions and restrictions of the ASM2 include the following. The heterotrophic and phosphate-accumulating biomasses are spatially homogenous and time-invariant. The internal structure of each individual cell is not distinguished and only an average composition is considered despite the use of nonlinear kinetic expressions. A pragmatic decision was made to accept the problems associated with the use of average biomass compositions as the introduction of population models would pose additional problems. The hydrolysis of organic matter, organic nitrogen, and organic phosphates are assumed to occur simultaneously in a coupled manner, and X_S comprises a constant fraction of nitrogen and phosphate. This is

a simplifying assumption to avoid the addition of 6 more hydrolysis process and 2 additional particulate components. Denitrification reactions of PAOs are not included in the model, though it is known that some PAOs can denitrify. Therefore, the model should be only used to simulate processes with low nitrate input into anaerobic tanks. The model assumes sufficient concentrations of phosphate, ammonia, potassium, and magnesium. The detailed mechanisms of growth limitations from low nutrient concentrations are not known and may not be accurately modeled. The effects of low potassium and magnesium concentrations on biological phosphorus removal are not considered. Finally, nitrate and nitrogen monoxide have been observed to inhibit biological phosphorus removal, but such effects are not incorporated in the model. Only critical assumptions that greatly affect the model performance are highlighted in this review. Other assumptions made in the ASM2 are detailed in the IWA ASM publication (Henze et al. 2000).

3.1.1.3. Activated Sludge Model No.2d (ASM2d)

The activated sludge model no. 2d incorporates the observation that PAO can use internal cell organic storage products for denitrification and thus grow under anoxic conditions. This observation is encompassed through the addition of two rate processes: the storage of polyphosphates and growth of PAO under anoxic conditions. All other details of the ASM2 carry over to the ASM2d.

3.1.1.4. Activated Sludge Model No.3 (ASM3)

With over 10 years of application of the ASM1, inaccuracies in the model had been identified, and the IWA task group worked to revise the ASM1 to resolve these

problems. The result is the activated sludge model no. 3, which appeared in 1999. One of the major changes in the ASM3 is the inclusion of internal cell storage compounds in heterotrophs. The focus is now shifted to the storage of organic substrates rather than hydrolysis. All readily biodegradable substrates are taken up by the hetertrophic biomass and stored as internal cell components prior to its growth. Thus, heterotrophic growth is not fully dependent upon external compounds. The inclusion of internal cell storage structure also leads to the distinction between the decay of biomass and storage products under both aerobic and anoxic conditions. Another significant difference is the replacement of the death-regeneration concept by the growth-endogenous respiration model. In the ASM1, the single concept of decay was represented by lysis and used to describe all decay processes although decay rates of nitrifiers and heterotrophs are generally different. In the ASM3, endogenous respiration is used to capture all forms of biomass loss and energy requirements, which are not associated with growth. The growth and decay of the two groups of organisms are clearly separated, as shown in Fig. 7, and identical models are used to describe the decay processes. These changes better reflect observed phenomena.

Components added to the ASM1 (in the ASM3) are dinitrogen, internal cell storage product of heterotrophic organisms, and suspended solids. Components in ASM1, no longer in ASM3, are particulates from biomass decay as well as soluble and particulate biodegradable organic nitrogen. The 13 components and 12 rate processes described in the model are listed in Table 2. Limitations of the model are as follows. The model was developed for domestic wastewater and, therefore, should not be used to

model treatment of industrial waters. It is applicable within the temperature range of 8-23°C and a pH range of 6.5-7.5, excluding anaerobic conditions. The model is not designed for systems with high loads and small SRT (<1 day) and cannot deal with high concentrations of nitrite.

3.1.1.5. Assessment of the Activated Sludge Models

The ASM1 has been tested extensively against experimental and operational data for activated sludge systems. Main problems found with the ASM1 have been addressed in the development of the ASM3. The ASM2, ASM2d, and ASM3 have also been validated against experimental data for conventional activated sludge systems, although less extensively so than the ASM1. It has been suggested that activated sludge models may be suitable for characterizing biomass kinetics in an MBR system. However, few studies have demonstrated the validity (or invalidity) of the ASMs for modeling MBR systems.

In a study by Wintgens et al. that introduces an integrated MBR model (Wintgens et al. 2003), simulation results from the ASM3, assuming steady-state conditions, were compared with averaged measured values for COD, ammonium, and nitrate plus nitrite from a full-scale operational MBR plant. The simulation results corresponded well with the measured data. Although the study implies that the ASM3 is a good modeling method for MBR systems, further in-depth studies are necessary to consider other components and transient states.

The applicability of the ASMs for modeling MBR systems needs to be verified to further understand effects of higher SRTs and MLSS concentrations on biomass. One of

the advantages of using the ASMs is its clear presentation in a matrix format. The matrix aids in the understanding of the biological treatment process and efficient experimental design. Another advantage is that many simulation programs include the ASMs or ASM-based models, providing easy access of the model for various applications. Also, biological phosphorous removal, which is a key feature in biological treatment, is already incorporated into the ASM2 and ASM2d.

3.1.2 Soluble Microbial Products (SMP) Model

While there are nuances among researchers as to what comprises soluble microbial products (SPM), SMP are generally defined as the organic materials arising from substrate metabolisms (usually with biomass growth) and biomass decay and are present in the effluent of biological systems but absent from the influent. Studies have shown that soluble microbial products comprise a considerable portion of soluble organic matter in the effluent of biological treatment processes, and the presence of SMP in the permeate is detrimental to treatment and post-treatment processes (Barker and Stuckey 1999). While it is still unclear whether the accumulation of SMP in the activated sludge inhibits metabolic activity, as contradicting results have been reported (Huang et al. 2000; Shin and Kang 2003), studies agree that build up of SMP can cause reduction in membrane permeability (Huang et al. 2000; Shin and Kang 2003; Park et al. 2005; Rosenberger et al. 2006). Additionally, SMP in the permeate stream can lead to formation of trihalomethanes and other disinfection by-products and cause bacterial growth in distribution systems (Furumai and Rittmann 1992). Hence, it is crucial to include SMP in the modeling of biological water treatment processes.

In 1992, Furumai and Rittmann presented a model that describes the interaction between heterotrophic and nitrifying bacteria in biological treatment processes (Furumai and Rittmann 1992). The model accounts for the formation and exchange of SMP between the two types of organisms, i.e., heterotrophs and nitrifiers, which are known to compete with each other for dissolved oxygen. Nitrifiers can also supply a potential energy for heterotrophs. They chemically reduce inorganic carbon into organic carbon in the form of cell mass and SMP and make organic substrates available for growth of heterotrophs.

In the model, SMP is divided into two groups: utilization associated products (UAP), which are produced in biomass growth, and biomass associated products (BAP), which arise from biomass decay. The two types of SMP are grouped together in the model, but their formation is accounted for separately. The formation rate of UAP is proportional to the substrate utilization rate, whereas the formation rate of BAP is proportional to the amount of active biomass. Both organisms produce SMP, but only heterotrophs degrade SMP for cell synthesis. A mass balance equation over the system was provided for each of the model components (organic COD, ammonium, nitrite, dissolved oxygen, nitrate, originally formed SMP, actual SMP, heterotrophs, ammonium oxidizers, nitrite oxidizers, and inert biomass).

The model was modified in 1998 to include features specific to the MBR process (de Silva et al. 1998; Urbain et al. 1998). Mainly, the output of biomass in the effluent was eliminated because the membranes retain the biomass in the system. The retention of a BAP fraction was also incorporated, as the fractions comprise of larger macromolecules

that are maintained in the reactor by membranes. Additionally, denitrification reactions were integrated into the model, and the biodegradation rates of the two types of SMP were modified according to recent findings that had suggested separate rates of UAP and BAP consumptions following Monod-type kinetics. The model includes 10 transient mass balance equations to characterize each constituent quantified in the model: heterotrophs, nitrifiers, inert biomass, soluble COD, ammonia, nitrate, nitrogen gas, oxygen, BAP, and UAP. As in the activated sludge models, the multiplicative Monod equations were used to capture rate limitations stemming from the deficiency of necessary substrates.

The SMP model demonstrated good correspondence between simulations results and measured data. In a study conducted by Urbain et al. (Urbain et al. 1998), a comparison was made between data from an MBR pilot plant with model predictions for oxygen demand, nutrient removal, sludge production, and biomass distribution under both steady and transient states at three different sludge ages. The model was not calibrated specifically for the pilot plant. Despite the use of default parameter values from literature, a good correspondence was found between model predictions and experimental values for VSS concentration, effluent COD, and nitrogen species. The model demonstrated the capability of producing accurate predictions under both steady and transient cases. The SMP model, however, could not handle technical problems during operation and sudden changes in the wastewater characteristics.

Another study was conducted by de Silva et al. involving another pilot-scale MBR (de Silva et al. 1998). Conditions were maintained at steady state, although the

aerated and anoxic periods in the system were alternated every two hours (i.e., 2-hour aerated period, 2-hour anoxic period). The pilot was operated at an HRT of 17 hours and SRT of 20 days. Most of the parameter values for the model were again taken from literature or computed stochiometrically. Comparison of the performance data and model simulation showed that the model was able to accurately predict the concentrations of sludge and nitrogen species and also capture general trends for the soluble COD in the effluent.

One of the advantages of the SMP model over the ASMs is its capability to accurately model biomass in MBRs without need for calibration using experimental data. It also involves less components and equations while still capturing key quantities and includes SMP fate. However, the model is not presented in a manner that facilitates ease of model application, and it does not incorporate the biological phosphorous removal.

3.1.3 ASM1-SMP Hybrid Model

Another model that incorporates the formation and degradation of SMP is a modified version of the ASM1 (Lu et al. 2001). Here, the same definition for SMP is used as in the SMP Model described above. The main concepts of the ASM1 are preserved in the hybrid model, but a few changes were made to include the SMP fate. A schematic description of the model that depicts these changes is provided in Fig. 8. UAP is released in the metabolic processes of autotrophs and heterotrophs, and heterotrophs can reutilize UAP for their growth. In addition to inert material and soluble substrates, the decay processes of the organisms produce BAP, which can also be reused for heterotrophic growth. These changes were incorporated as follows. The component X_P,

particulate products arising from biomass decay, was replaced with BAP and UAP. Process rates for aerobic and anoxic growths of heterotrophs from SMP consumption were added. Additionally, the decay rates of the two organisms were separated into two processes, i.e., one resulting in particulate formation and another resulting in BAP formation. The stoichiometric coefficients were adjusted accordingly with the inclusion of these rate processes. The model comprises 12 transient mass balance equations, and alkalinity is not considered.

Experiments were carried out with a single completely-mixed bioreactor that treated synthetic wastewater to test the validity of the AMS1-SMP hybrid model. The MBR was operated with aerobic and anoxic cycling of 60 minutes (30 minutes with aeration, 30 minutes without aeration) and 120 minute cycles (60 minutes with aeration, 60 minutes without aeration). Most original parameters of the ASM1 were used, but the denitrification correction factor was enhanced to account for higher sludge concentrations in the system. Parameter values arising from the modification to include SMP were determined by trial and error or obtained from references. The model simulation results showed good correspondence for soluble COD and soluble nitrogen concentrations under steady-state conditions. However, MLSS concentrations were significantly underestimated for both cycling conditions. The ASM1-SMP hybrid model is a first attempt at modifying the ASMs to model MBRs. Modifications are made based on research that suggested the importance of the inclusion of SMP components for activated sludge with high SRTs. The incorporation of SMP into the ASM1 takes advantage of

some benefits of the ASM and SMP models, though more work is needed to fine-tune the hybrid model.

3.1.4 Empirical Hydrodynamic Model

To investigate the influence of hydrodynamic conditions on the mixed liquor cross-flow velocity and the membrane fouling rate in an MBR, 10 experiments were performed at varying suspended solid (SS) concentrations (X, 2-20 g-L^{-1}), permeate fluxes (J, 4.5-27 L-m^{-2}-h^{-1}), and aeration intensities (U_{Gr}, 10-100 m^3-m^{-2}-h^{-1}) in an internal-loop-airlift reactor (Liu et al. 2003). The reactor is shown in Fig. 9. Air is supplied only in the riser zone of the reactor, which is separated from the down-comer sections by baffle plates. The air hold-up in the riser section results in a difference in the bulk density of the liquid, inducing circulation between the two zones. The cross-flow velocity is an important factor to consider in impeding sludge buildup on the membrane surface.

Over the duration of each experiment, the up-flow velocity of the mixed liquor in the riser zone (U_{sr}, m s^{-1}) and the transmembrane pressure (ΔP, Pa) were monitored. The up-flow velocity was measured as an observable value of the actual cross-flow velocity of the mixed liquor along the membrane surface. Note that the aeration intensity, U_{Gr}, is distinct from the mixed liquor cross-flow velocity, U_{sr}. The former is a controlled parameter in the experiment, whereas the latter is a measured value that is influenced by controlled parameters. The transmembrane pressure was used to calculate the membrane fouling rate (K, m^{-1}-h^{-1}), defined as the rate of increasing membrane

filtration resistance (i.e., $K = \mathrm{d}R/\mathrm{d}t$). The following equation was used to compute the filtration resistance (R, m^{-1}):

$$R = 3.6\times10^{9}\frac{\Delta P}{\eta J} \tag{32}$$

Here, η (mPa-s) is the viscosity of the permeate and was approximated with the viscosity of tap water. The factor, 3.6×10^{9}, stems from using the units given in parentheses for each of the variables. The membrane resistance over time was plotted for each experiment, and the membrane fouling rate was obtained from the slope of the linear regression through the plot. Correlations were developed from the experimental data for the mixed liquor cross-flow velocity and the membrane fouling rate as functions of the hydrodynamic parameters.

The aeration intensity, reactor structure, and fluid viscosity were regarded to be the main factors influencing the mixed liquor cross-flow velocity. The correlation for the cross-flow velocity was assumed to fit the following power equation:

$$U_{sr} = f_1 U_{Lr}^{a}\mu^{b} \tag{33}$$

Here, U_{Lr} (m-s^{-1}) is the cross-flow velocity of tap water, μ is the mixed liquor viscosity (mPA-s), and f_1, a, and b are constants. U_{Lr} was found by measuring up-flow velocity of just tap water in the reactor. The parameter was used to capture the combined influence of the aeration intensity and reactor structure, since the reactor structure affects the sludge cross-flow velocity but is not a directly quantifiable parameter. Multiple regression analysis was used to determine the value of the three constants. The

relationship between sludge viscosity and SS concentration was established from the experimental data:

$$\mu = 1.61e^{0.07X} \tag{34}$$

and was used to replace μ in Eq. (33) to obtain U_{sr} in terms of X. The following was given as the final equation for the mixed liquor cross-flow velocity:

$$U_{sr} = 1.311U_{Lr}^{1.226}e^{-0.0105X} \tag{35}$$

Key factors influencing the membrane fouling rate were considered to be the aeration intensity (again captured by the tap water cross-flow velocity to incorporate the effect of the reactor structure), permeate flux, and suspended solids concentration. The parameters were fitted to the power equation:

$$K = f_2 U_{Lr}^{c} J^{d} X^{e} \tag{36}$$

where f_2, c, d, and e are constants. The values of these constants were determined using the least squares method: $f_2 = 8.933\times10^7$, $c = -3.047$, $d = 0.376$, and $e = 0.532$. These two equations, for U_{sr} and K, are supplied to quantitatively characterize membrane fouling in an MBR.

The equations supplied by the hydrodynamic model explicitly show the correlation of various hydrodynamic parameters to two important factors, the membrane fouling rate and mixed liquor cross-flow velocity. The mixed liquor cross-flow velocity is significant because it gives insight into the impact of hydraulic conditions on membrane fouling in terms of the retardation of sludge accumulation on the membrane surface. While the model is very easy to use, it is too simple to capture the complicated

phenomena on the membrane surface and fails to account for many other conditions and operational parameters. Consequently, the model was unable to accurately reproduce the experimental results from which it was derived for the membrane fouling rate. The calculated mixed liquor cross-flow velocities corresponded well with the measured values. However, it must be tested against a different set of experimental data to support its validity. In general, the model may be useful for illustrating the relative weighting of the effect of certain hydrodynamic conditions on membrane fouling, but its application for operational and design purposes is questionable.

3.1.5 Fractal Permeation Model

A permeation model, based on fractal theory and Darcy's law, was developed by Meng et al. to evaluate the permeability of cake formed from the microfiltration of activated sludge (Meng et al. 2005). The microstructure of a cake layer is usually disordered and complicated, and thus, cannot be described by traditional geometry. Fractal theory can be applied here to characterize the irregular object in terms of its average self-similar properties. The authors first introduce a fractal model to determine the pore area fractal dimension, D_s, of a cake layer:

$$B(\geq a) = S_c - A = C_0 (a)^{2-D_s} \tag{37}$$

where a is a threshold pore area, B is the total cake layer area (S_c) minus the sum (A) of all pore areas equal to or larger than a (i.e., $A = \sum a$), and C_0 is a constant. This model stems from a fractal model developed by Kaye et al. (Kaye 1994; Xu et al. 1995). The authors provide a procedure for physically determining the fractal dimension of a

cake layer, which involves the use of an image analyzer to evaluate each pore area. Eq. (37) can be applied to calculate the values of B from several defined threshold values of a. The fractal dimension can then be computed from the slope of the straight-line through the plot of $\ln B$ vs. $\ln a$.

The permeability model was derived by modifying the Hagen-Poiseulle equation for flow rate through a tortuous capillary or pore {Yu, 2004 #27}. The equation was rewritten in terms of the threshold pore area, a, rather than the pore diameter, λ:

$$q(a) = \frac{G}{g}\frac{\Delta P}{L(a)}\frac{a^2}{\mu} \tag{38}$$

Here, G is the geometry factor for fluid flow through a pore (i.e., $\pi/128$ for circular pores), g is the shape factor where $a = g\lambda^2$, ΔP is the pressure gradient, $L(a)$ is the tortuous length of a pore, and μ is the dynamic viscosity. Straight pores were assumed in the cake layer, allowing the replacement of $L(a)$ by a constant L_0. A unit flow rate was obtained by dividing Eq. (38) by a, and the flow rate through an area $\mathrm{d}A$ was expressed as:

$$\mathrm{d}Q = -\frac{q(a)}{a}\mathrm{d}A = -\frac{G}{g^2}\frac{\Delta P}{L_0}\frac{a}{\mu}\mathrm{d}A \tag{39}$$

The portion of cake area, $\mathrm{d}A$, was obtained by taking the derivative of Eq. (37) with respect to a:

$$\mathrm{d}A = -C_0(2 - D_s)a^{1-D_s}\mathrm{d}a \tag{40}$$

Combining Eqs. (39) and (40) and integrating over the pore area distribution range ($a_{\min}$ to $a_{\max}$) gave:

$$Q = C_0 \frac{G}{g^2} \frac{\Delta P}{L_0} \frac{1}{\mu} (2 - D_s) \int_{a_{\min}}^{a_{\max}} a^{2-D_s} \mathrm{d}a$$
$$= \frac{G}{g^2} \frac{\Delta P}{L_0} \frac{1}{\mu} C_0 \frac{2 - D_s}{3 - D_s} \left(a_{\max}^{3-D_s} - a_{\min}^{3-D_s} \right) \tag{41}$$

Eq. (41) was reduced to

$$Q = \frac{G}{g^2} \frac{\Delta P}{L_0} \frac{1}{\mu} C_0 \frac{2 - D_s}{3 - D_s} a_{\max}^{3-D_s} \tag{42}$$

by recognizing that the fractal dimension must be between 1 and 2 and that $a_{\max}$ is much greater than $a_{\min}$ (i.e., $1 < D_s < 2$, so $3 - D_s > 1$ and $a_{\max} \gg a_{\min}$, so $a_{\max}^{3-D_s} \gg a_{\min}^{3-D_s}$). The expression for the flow rate, Q, in Eq. (42) was substituted into Darcy's law to obtain the following equation for the permeability of porous cake:

$$K = \frac{\mu L_0 Q}{\Delta P A_t} = \frac{G}{g^2} C_0 \frac{1}{A_t} \frac{2 - D_s}{3 - D_s} a_{\max}^{3-D_s} \tag{43}$$

The authors defined a cake layer permeation factor, K':

$$K' = \frac{2 - D_s}{3 - D_s} a_{\max}^{3-D_s} \tag{44}$$

which they used to illustrate the validity of their model. A number of membrane fouling experiments were performed with varying activated sludge properties. The specific resistance of the cake layer development (r_c) in each experiment was determined indirectly. The inverse of the specific cake resistance is equal to cake permeability, and therefore, the plot of the permeation factor against $1/r_c$ should show high linearity if the

model is valid. A correlation coefficient of 0.857 for the linear regression was observed. Based on this, the authors asserted that the model is reasonable to some degree and is valid in theory.

The fractal permeation model provides a method for determining the permeability of cake buildup on a membrane surface. The model involves only a few parameters that are fairly easy to determine and does not require intensive computation to solve. However, the validity of the model has only been somewhat implied by experiment and has not been directly verified. More adequate verification is necessary to determine the model's applicability. The model does not show how operational parameters and conditions affect the cake resistance, but relies on the fractal dimension to capture different effects. Therefore, various parameters must be correlated with the pore area fractal dimension (or permeation factor) to determine their effect on the cake resistance.

3.1.6 Sectional Resistance Model

In a submerged MBR, coarse bubbles from aeration provide an additional cleaning mechanism for the immersed membrane modules by scouring the membrane surface. This shear force from aeration is unevenly distributed, resulting in non-uniform fouling. Li and Wang apply a sectional approach to account for the uneven cake formation in determining the total filtration resistance on a membrane surface (Li and Wang). They divided the membrane surface into equal fractional areas, $\Delta\varepsilon$, and calculated a separate total resistance, R, in each section. The total resistance in each section is the sum of the resistance components in the section:

$$R = R_m + R_p + R_{sf} + R_{sc} \tag{45}$$

Here, R_m is the inherent membrane resistance. R_p is the pore fouling resistance. It is proportional to the amount of permeate produced and is given by

$$R_p = r_p \sum J\theta_f \tag{46}$$

where r_p is the specific pore fouling resistance, J is the permeate flux, and θ_f is the filtration period of an operation cycle. R_{sf} is the resistance due to dynamic sludge film and is the product of the specific resistance of the biomass in the dynamic film, r_{sf}, and the mass of the dynamic sludge film, M_{sf} (i.e. $R_{sf} = r_{sf}M_{sf}$). Likewise, the resistance of the stable sludge cake layer, R_{sc}, is equal to the product of the specific resistance of the sludge cake layer, r_{sc}, and the amount of biomass accumulated on the membrane surface, M_{sc} (i.e. $R_{sc} = r_{sc}M_{sc}$).

The mass of the sludge in the dynamic film can be determined from the following equation during the filtration period:

$$\frac{dM_{sf}}{dt} = \frac{24CJ^2}{24J + C_d d_p G} - \frac{\beta(1-\alpha)GM_{sf}^2}{\gamma V_f t + M_{sf}} \tag{47}$$

The first and second terms of Eq. (47) represent the rate of attachment and detachment, respectively. The attachment rate was derived by considering the opposing forces (i.e., the drag force that leads to attachment and a lift force caused by turbulence) acting on a particle as it approaches the membrane. The probability of the deposition of the particle on the membrane surface is given by the attachment force divided by the sum of the two forces. Multiplying this probability by the mass flux (the sludge concentration times the permeate flux) gives the rate of attachment. Here, C is the sludge concentration, J is the

local permeate flux in the membrane section, C_d is coefficient of the lifting force of a sludge particle of diameter d_p, and G is the shear intensity on the section of the membrane surface. The detachment rate was assumed to follow a first order kinetic process ($\left(\mathrm{d}M_{sf}/\mathrm{d}t\right)_d = -K_d M_{sf}$). The rate coefficient, K_d, was thought to vary with the mass of the sludge film. It increases with M_{sf} and reaches a maximum for large values of M_{sf}. Therefore, it was proposed to have the form of a Monod equation ($K_d = \frac{\kappa_r M_{sf}}{\kappa_s + M_{sf}}$). Expressions were assumed for the maximum rate constant, κ_r, and half-saturation constant, κ_s. In the detachment rate expression, β is the erosion rate coefficient of the dynamic sludge, α is the stickiness of biomass particles, γ is the compression coefficient for dynamic sludge, V_f is water production within the filtration period of operation cycle, and t is the filtration time. During the cleaning period, no attachment occurs, and the rate of detachment is given by

$$\frac{dM_{sf}}{dt} = -\frac{\beta(1-\alpha)GM_{sf}^2}{0.1\gamma V_f \theta_f + M_{sf}} \tag{48}$$

which is just 10 times the detachment rate given in Eq. (47). The factor 0.1 in the denominator arises from the presumption that the compression coefficient is reduced during the cleaning period by a tenth of its original value. The remaining sludge after cleaning, ΔM_{sc}, adds to the stable sludge cake layer.

For the shear intensity, G, at each section, the following shear profile was assumed:

$$\frac{G}{G_0}=\begin{cases}\frac{1}{10}+\frac{9}{20}\left[1+\sin\frac{(2\varepsilon_i-\varepsilon_a)\pi}{2\varepsilon_a}\right] & \varepsilon_i<\varepsilon_a \\ 1 & \varepsilon_i\geq\varepsilon_a\end{cases} \tag{49}$$

Here, G_0 is the apparent shear intensity of the fluid turbulence, ε_i is the accumulated membrane area fractions up to the ith section, and ε_a is the sectional area of membrane surface with reduced shear intensity (where G/G_0 is less than 1).

The sectional resistance model was developed using a partially analytic approach. The model is intended to characterize membrane fouling in submerged MBRs where the membranes are subjected to shear from aeration. In dividing the membrane into sections and considering the resistance in each section, the model accounts for in uneven cake formation stemming from uneven shear distribution along the membrane surface. The advantages of this transient model are that it accounts for cleaning cycles and characterizes fouling development over time. The experiment was conducted using a submerged MBR, which filtered a glucose based synthetic wastewater with varying sludge concentrations, filtration fluxes, and aeration intensities. Comparison of the measured and computer simulated TMP over MBR operation time revealed that the model is only able to capture very general trends and is not suitable for applications requiring accurate modeling of membrane fouling.

3.1.7 ASM1-SMP Hybrid and Resistance-In-Series Model

An integrated MBR model was presented by Lee et al. in which the ASM1 was modified to include components for SMP and additional rate processes to describe SMP

fate (Lee et al. 2002). The resistance-in-series model was adapted to account for the influence of the biomass on membrane fouling. Much like the ASM1-SMP hybrid model presented by Lu et al. (Lu et al. 2001), four rate process expressions (slightly different from the ASM1-SMP hybrid model described earlier) were added to the ASM1. The model stochiometry was accordingly modified. The four processes are listed below.

Aerobic growth from S_{SMP}:

$$\mu_{SMP}\frac{S_{O_2}}{K_{O_2}+S_{O_2}}\frac{S_{SMP}}{K_{SMP}+S_{SMP}}\frac{S_{NH_4}}{K_{NH_4}+S_{NH_4}}\frac{S_{ALK}}{K_{ALK}+S_{ALK}}X_H$$

Anoxic growth from S_{SMP}:

$$\mu_{SMP}\eta_{NO_3}\frac{S_{SMP}}{K_{SMP}+S_{SMP}}\frac{K_{O_2}}{K_{O_2}+S_{O_2}}\frac{K_{NO_3}}{K_{NO_3}+S_{NO_3}}\frac{S_{NH_4}}{K_{NH_4}+S_{NH_4}}\frac{S_{ALK}}{K_{ALK}+S_{ALK}}X_H$$

Lysis of heterotrophic organisms producing S_{SMP}: $b_{H,SMP}X_H$

Lysis of autotrophic organisms producing S_{SMP}: $b_{A,SMP}X_A$

The main difference between this and the previously described ASM1-SMP hybrid model is that this model still accounts for alkalinity, and the influence of alkalinity and ammonia concentrations on the heterotrophic growth rates is incorporated into the additional process rate expressions. The previously described hybrid model does not consider alkalinity and removes ammonia concentration limitations on the growth rates of heterotrophs.

To model membrane fouling, the following equation for the total filtration resistance was supplied:

$$R = R_m + m\alpha \tag{50}$$

where

$$m = k_m \frac{V_p X_{TSS}}{A} \tag{51}$$

Here, R_m is the membrane resistance, α is the specific resistance, k_m is a coefficient ranging from 0 to 1 to reflect cross-flow filtration effects (e.g. $k_m = 1$ for dead-end filtration), V_p is the permeate volume, X_{TSS} is the concentration of total suspended solids (TSS) in the biomass, and A is the membrane surface area. SMP was not considered in the membrane resistance since its concentration was thought to be negligible compared to the TSS concentration.

The resistance model given here involves few parameters for predicting the total resistance on the membrane surface. The parameter values can be easily determined, and the total resistance is simple to calculate. However, both the biomass kinetics and resistance models have not been validated, and the applicability of the models is unknown.

3.1.8 ASM3 and Resistance-In-Series Model

In the study by Wintgens et al. (Wintgens et al. 2003), a model was introduced to describe the filtration performance of submerged capillary hollow fiber modules in an MBR. The model was combined with the ASM3 to describe the biological treatment process. It was acknowledged that extra-cellular polymeric substances (EPS) produced by

the microorganisms can hamper membrane performance, but no modifications were made to the ASM3 to quantify this component.

In the model, the permeate flux was given as

$$F = \frac{\Delta p_{TM}}{\eta_P \left(R_M + R_C + R_F \right)} \tag{52}$$

where

$$\Delta p_{TM} = p_{hydro} + p_{pump} - \Delta p_{ax} \tag{53}$$

The effective trans-membrane pressure difference, Δp_{TM}, is the sum of the hydrostatic pressure, p_{hydro}, and the suction pressure, p_{pump}, minus the pressure loss from permeate flow along the hollow fibers, Δp_{ax}. The total resistance is the sum of the membrane resistance, R_M, the cake resistance, R_C, and the fouling resistance R_F. The cake resistance is given by

$$R_C = k_C c_M \tag{54}$$

where

$$c_M = c_b e^{F(t)/k_P} \tag{55}$$

and

$$k_P = \frac{\tau_W d_C}{\eta_F} \tag{56}$$

Here, k_C is the cake layer model parameter, c_M is the concentration at the membrane surface, c_b is bulk concentration, $F(t)$ is the trans-membrane flux, k_P is the local mass

transfer coefficient, τ_W is the mean wall shear stress, d_C is characteristic particle diameter, and η_F is viscosity of the activated sludge. The fouling resistance was given as

$$R_F = S_F\left(1 - e^{-k_F\int_0^t F(t)dt}\right) \tag{57}$$

where S_F is a model parameter for fouling saturation, k_F is a model parameter for fouling, and $\int_0^t F(t)dt$ is the total permeate volume per membrane area produced between two chemical cleanings. The final form of the permeate flux is an implicit expression:

$$F(t) = \frac{p_{hydro} + p_{pump} + \Delta p_{ax}}{\eta_P\left(R_M + k_C c_b e^{F(t)/k_P} + S_F\left(1 - e^{-k_F\int_0^t F(t)dt}\right)\right)} \tag{58}$$

This model is based on the resistance-in-series model and was developed to describe the filtration performance of submerged capillary hollow fiber modules in an MBR. Like the sectional resistance model, this model accounts for cleaning cycles, and time dependency is incorporated into the model to provide a continuous fouling profile. The model was tested against operational data from a full-scale MBR with two external filtration units. Data from the first unit was used to set model parameters by curve fitting using the least-square-error method. Simulation results from calibrated model were then compared with data from the second filtration unit. Except for the initial period of operation, the computed permeability over time corresponded well with measured data. The model has also been validated with experimental data from a pilot MBR with submerged capillary hollow fiber membranes (Geissler et al. 2005). The simulation results for the permeability evolution over time matched well the data from the pilot plant

except for a major deviation at the end of the considered period. The deviation was explained by a drop in the organic load in the influent that was not considered in the simulation.

3.2 Core MBR Model Components and Parameters

For any given wastewater treatment system, of primary concern are the effluent quality that the system is capable of achieving and the investment and operating costs of the system. The system must be able to treat the water to meet water quality standards as set forth by regulatory agencies, and it must, simultaneously, be economical. Model development should, therefore, center on components for which water quality standards have been set and on parameters that are strongly correlated to cost. A few key model components and parameters for MBRs are given here.

3.2.1 Resistances

The permeate flux and transmembrane pressure are directly related to costs. The two parameters are correlated by the permeate viscosity and total resistance. The ability to quantify the individual resistance (i.e., resistance from cake formation and adsorptive fouling) as a function of the various influencing parameters is important in determining what parameters have the greatest effect on fouling, for designing system and operating conditions, and for optimizing the system to achieve an economical balance between production and applied pressure. Parameters that affect fouling include sludge concentration, shear rate, concentration of pore-blocking and membrane adsorptive materials in the feed, and membrane properties.

3.2.2 Biomass (MLSS) Concentration

MBRs typically operate at higher biomass concentrations than conventional biological treatment processes. The advantage that this provides is increased volumetric loading and less sludge production, which lowers capital investment costs for civil works and reduces sludge disposal costs. However, higher biomass concentrations can adversely affect membrane performance, necessitating increased membrane area and, thus, increasing investment costs. Biomass concentration also influences energy costs. There is reduced oxygen transfer rate associated with higher biomass concentrations, so energy cost for aeration increases with increasing biomass concentration. Additionally, the greater the biomass concentration, the higher the sludge viscosity, which requires a larger applied pressure to achieve a certain permeate production rate. Determining the relationship between biomass concentration and other parameters can aid in identifying an optimal biomass concentration for operation, which can lead to significant economical savings.

3.2.3 Dissolved Oxygen Requirement and Oxygen Transfer Rate

Aeration accounts for a significant portion of energy costs in the operation of MBR systems. Thus, optimizing the oxygen supply can favorably affect operating costs. Determining the dissolved oxygen requirement and the conditions to supply sufficient oxygen at a high oxygen transfer rate can reduce wastage of oxygen. Some of the factors that influence the oxygen transfer rate include the MLSS concentration, the MBR configuration, the type of bubbles used (fine or course), and the specific air flow rate. The

oxygen requirement depends on the constituents in the wastewater, the biomass concentration, and the biomass growth rates.

3.2.4 Carbon and Nutrient Concentrations

It is important to include carbon and nutrient (nitrogen and phosphorous components) concentrations in MBR models given that MBR process performance is characterized by these components. COD, BOD, ammonia/ammonium, nitrate/nitrite, and ortho-phosphate concentrations in the effluent should be captured by the model. The concentration of these components are affected by the concentration of the various types of organisms performing the removal of a certain component, the growth rates of these organisms, and the concentration of oxygen present in the system.

3.2.5 SMP

SMP comprises a major portion of the organic matter in effluents from biological treatment processes. It is important to quantify and minimize SMP in the effluent because they are possible precursors to trihalomethane and other disinfection by-products, competitively adsorbed by activated carbon, and can lead to biological growth in distribution systems. Additionally, EPS, which is a form of SMP that surrounds the surfaces of microorganisms, contributes to membrane fouling. Factors influencing the formation of SMP include the biomass concentration, loading rates, and sludge age.

3.3 Suggestions for Future Development

Suggestions for future work are discussed in the following sections. Preliminary work includes communication with practitioners and validation of existing models.

Integrating MBR models and examining other modeling approaches, namely the application of neural networks, are other areas of future work.

3.3.1 Survey of Practitioners

Full-scale operational MBR wastewater treatment plants have been designed and implemented all over the world. Useful information on the MBR models can be gleaned from the design process of these plants. A survey among the consulting companies and MBR manufacturers that design and supply the MBR systems can be conducted to determine what models are being used for the design process. Data can also be gathered from operational MBR plants to evaluate the performance of these models. Such a study could provide valuable data on the modeling of MBR systems, and an understanding of model needs, in a practical sense, can be gained.

3.3.2 Model Validation

Several of these models reviewed in this study have not been validated or are inadequately validated for MBR processes, namely the activated sludge models, the fractal permeation model, and the Lee et al. ASM1-SMP hybrid and resistance-in-series models. These models must be verified with experimental data to determine their applicability for modeling MBR systems. Validation studies not only serve the purpose of validating the model, but they can also provide insight into the MBR process. In particular, the verification of the ASMs can shed light into the effects that changes in MBR systems from conventional ASP have on biomass kinetics.

3.3.3 Integration of Biomass Kinetic and Membrane Fouling Models

Models that describe the biomass kinetics and membrane fouling in an MBR have been developed separately. However, processes in the biomass affect fouling on the membrane surface. Two of the papers in the review present integrated models (Lee et al. 2002; Wintgens et al. 2003). They introduce separate models that are slightly coupled to describe both processes. In the study by Lee et al., it was recognized that the biomass and SMP concentrations affect the resistance build up on the membrane surface, and the biomass concentration is incorporated in the calculation of the resistance buildup on the membrane surface. Wintgen et al. acknowledged that biomass properties and biomass metabolism and decay product affect membrane fouling, and they include parameters in their resistance-in-series model to capture some of these effects. However, these parameters are calibrated rather than linked with biomass transformation processes, so the model is not truly integrated. Applying an integrated approach in future MBR model development is recommended. For example, extra-cellular polymeric substances (EPS) are recognized to significantly affect membrane fouling. Therefore, biomass kinetic models should include a component for EPS, which can be used as a parameter for the characterization of membrane fouling.

3.3.4 Alternative Modeling Approaches: Artificial Neural Networks

Generally, existing models have employed coupled transient mass-balance equations to quantify components in the biomass and the conventional resistance model to describe membrane fouling. Other modeling methods can be examined, such as the application of artificial neural networks (ANN). ANN is an empirical model that must be

trained with pattern data to be able to predict an output parameter from a given set of inputs. They have been used successfully in many applications, including the prediction of colloidal fouling of membranes. One of the main advantages of this approach is that it does not require governing equations to describe the complex phenomenon of MBR processes. Studies have begun to look into ANNs to model membrane fouling in an MBR. In a study by Geissler et al. (Geissler et al. 2005), an Elman network was used to predict permeability from a set of measurable influencing parameters. Good correspondence was found between the predictions from the ANN model and measured data. ANNs can be potentially applied to model biomass kinetics in MBRs.

CHAPTER 4. CONCLUSION

Accurate and practical models for describing membrane processes are valuable tools that can contribute to furthering membrane technology. Two less-developed areas of membrane process modeling were examined in this study: the characterization of polydispersed colloidal fouling and membrane bioreactor systems. It has been shown that a porous medium of polydispersed particles can be represented by a medium of monodispersed particles with an effective radius of $a_{\text{eff}} = \sqrt{\langle a^3 \rangle / \langle a \rangle}$. Based on this concept, expressions were derived for the permeability of cake composed of particles with normal (Gaussian) and log-normal size distributions. Comparison of the two permeability expressions with identical mean and standard deviation values demonstrated that the medium with normally distributed particle sizes always exhibits a lower permeability (i.e., higher specific cake resistance) than that with log-normally distributed particle sizes. This lower permeability stems from the greater number of smaller particles in the normal distribution, which contribute significantly to a higher overall cake resistance. The comparison holds greater validity when the mean particle size is larger than 2 standard deviations. In the derivation of the permeability expressions, an important assumption made is that the particles all occupy an equal spatial fraction of volume. The equations are, therefore, more applicable when isotropic, random Brownian motion is dominant and less so when unidirectional shear-induced diffusion is significant.

Diffusion effects with different sizes of particles are less prominent in the former case than in the latter and, thus, a less stratified cake is formed.

A review of modeling studies on MBR application for municipal wastewater was conducted to assess current MBR modeling efforts. Models describing the biomass kinetics in an MBR include the activated sludge model family (ASM1, ASM2, ASM2d, and ASM3), the soluble microbial products model, and the ASM1-SMP hybrid model. The ASMs were developed to model the activated sludge process, and their ability to describe the MBR process has not been verified by in-depth experiments. Researchers suggest that SMP are important components in describing biomass kinetics due to the high SRT in MBR systems. Accordingly, the SMP model demonstrated the capability of characterizing the biomass in MBR systems with a reasonable to high degree of accuracy. A modified version of the ASM1 to incorporate SMP demonstrated good accuracy in quantifying COD and soluble nitrogen concentrations, but significantly underestimated MLSS concentrations. Further testing is needed to contribute to model development.

The membrane fouling models include the empirical hydrodynamic model, fractal permeation model, sectional resistance model, and the two resistance-in-series models presented as a part of integrated models. The empirical hydrodynamic model is too simple to describe the membrane fouling phenomenon, and the sectional resistance model lacks accuracy. Both the resistance-in-series model by Lee et al. and fractal permeation model have not been adequately verified by experiments. The resistance-in-series model developed by Wintgens et al. shows the most promise, as it is fairly accurate, accounts for cleaning cycles, and can predict permeability changes over time. Further tests are needed

to determine the universality of the model's parameters for MBR systems having different configurations and treating wastewaters with different characteristics.

Components and parameters that should be most accurately modeled were identified. They include cake and fouling resistances, biomass concentration, oxygen requirements and oxygen transfer rate, carbon and nutrient concentrations, and SMP concentration. These components and parameters indicate the performance of the system and are strongly correlated to investment and operating costs. For future work, communication with practitioners is suggested to identify the models that are currently being used in the design of MBR wastewater treatment plants and to assess the performance of these models. Several of the existing models, particularly the ASMs, require validation to determine their applicability for modeling the MBR process and to evaluate whether they can serve as a base for future model development. Membrane fouling in MBRs is affected by the biotransformation processes in the system. Therefore, the integration of biomass kinetics models and membrane fouling models for MBRs is suggested. Finally, examination of other modeling approaches, such as the application of artificial neural networks, is recommended, as they may provide better predictions of MBR performance.

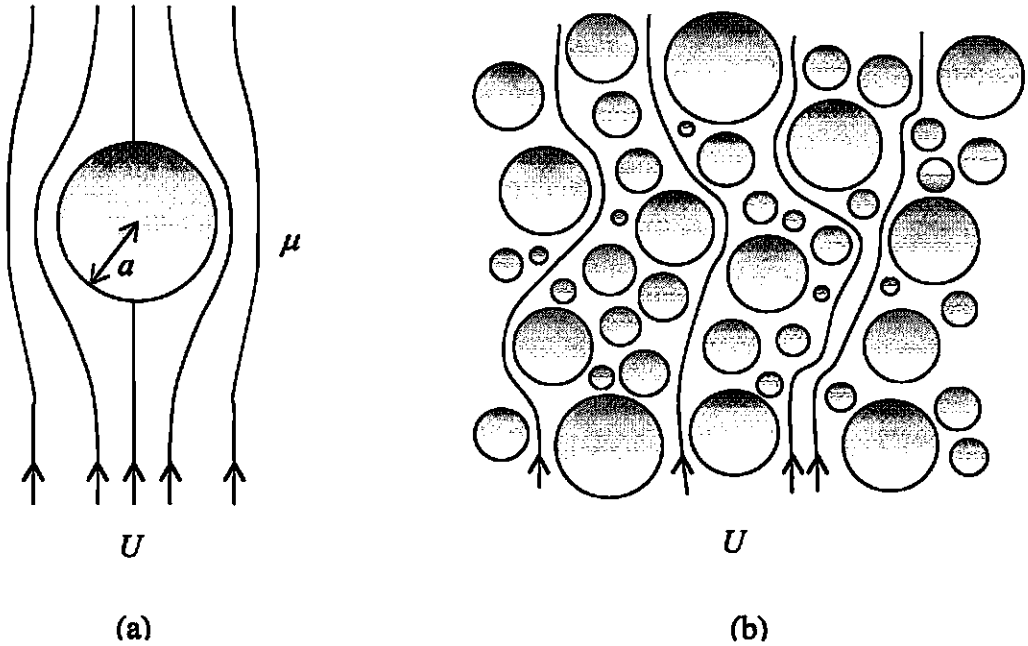

Fig. 1. Flow field (a) around a single spherical particle and (b) through a swarm of polydispersed particles

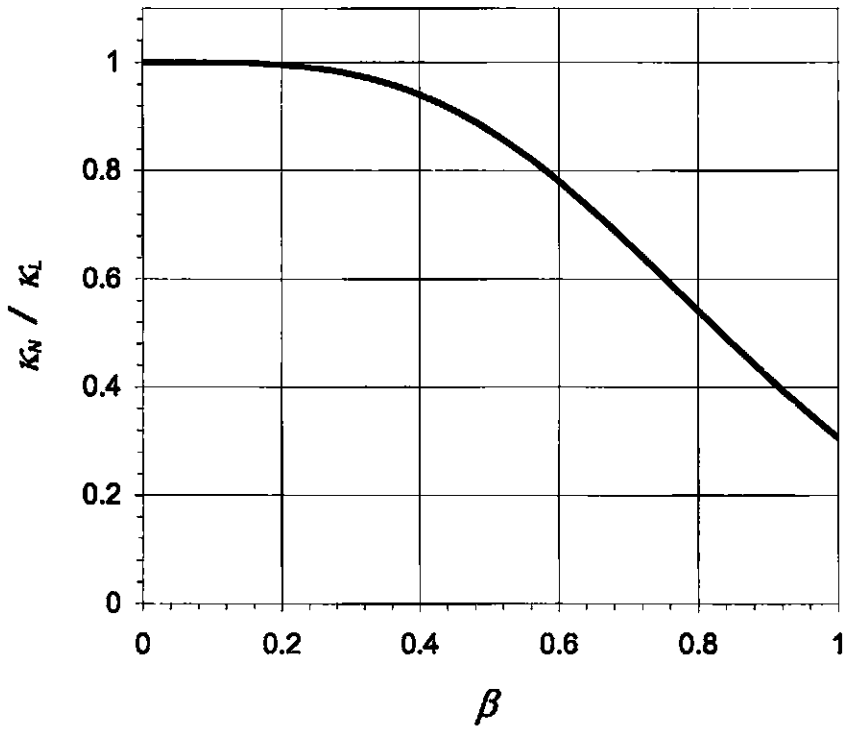

Fig. 2. Ratio of the normal to log-normal permeability as a function of β.

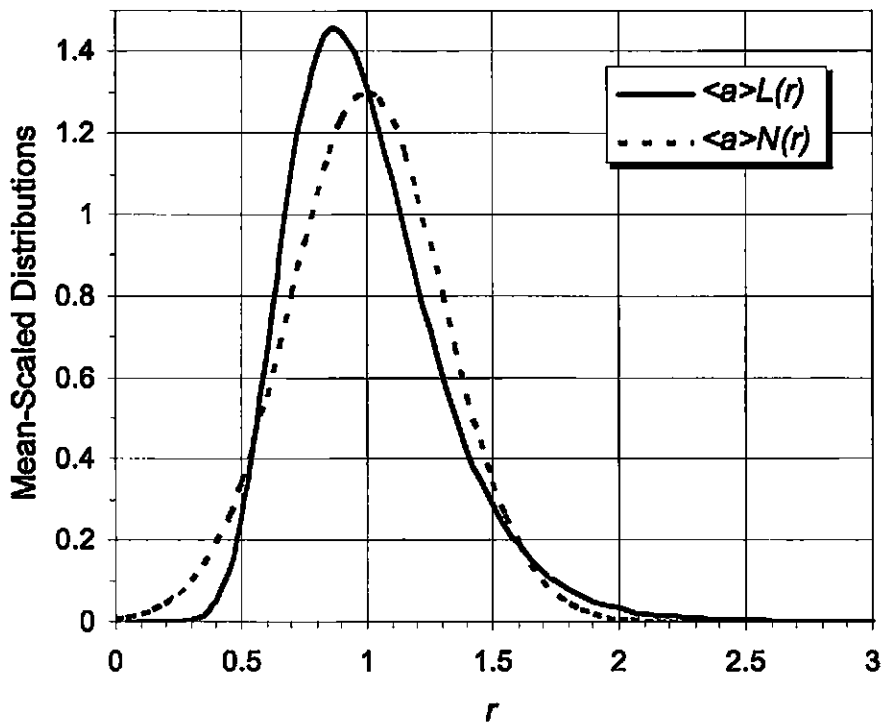

Fig. 3. Mean-scaled log-normal $(\langle a\rangle L(a))$ and normal $(\langle a\rangle N(a))$ distributions as a function of $r(=a/\langle a\rangle)$ with $\beta = 0.3$.

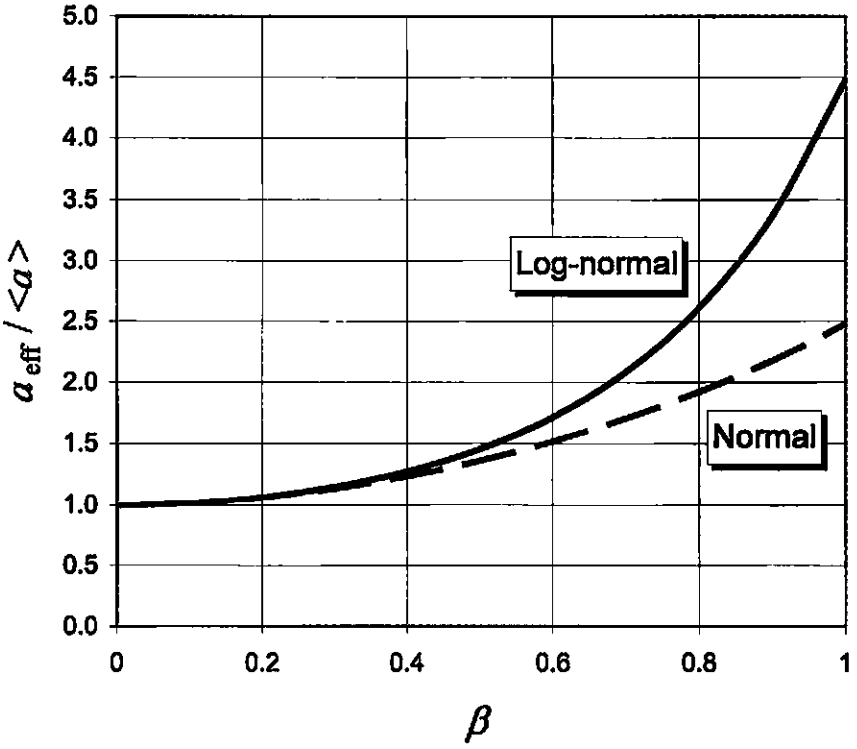

Fig. 4. Dimensionless effective radius $a_{eff} / \langle a \rangle$ of log-normal and normal distributions as a function of β.

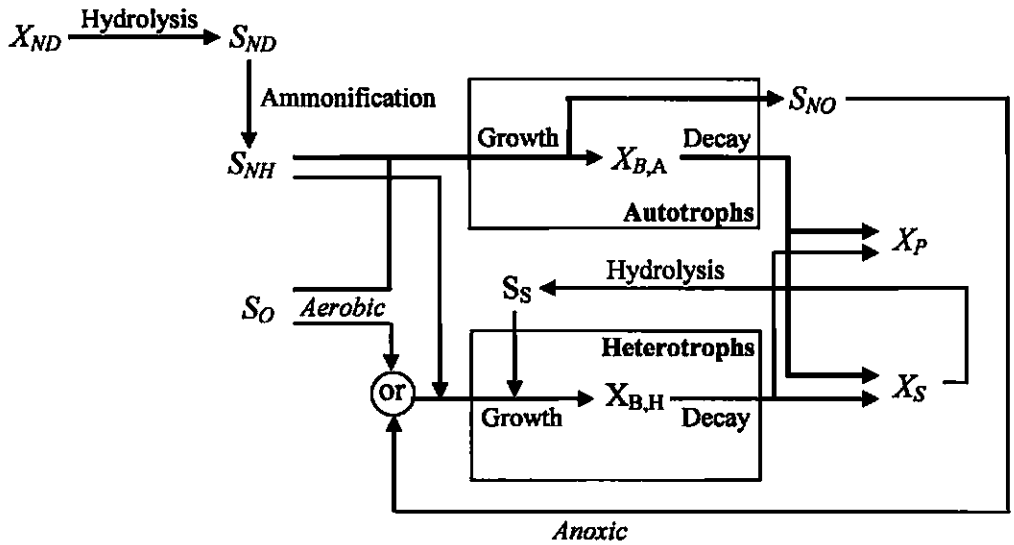

Fig. 5. Diagram of model processes and substrate flow in ASM1

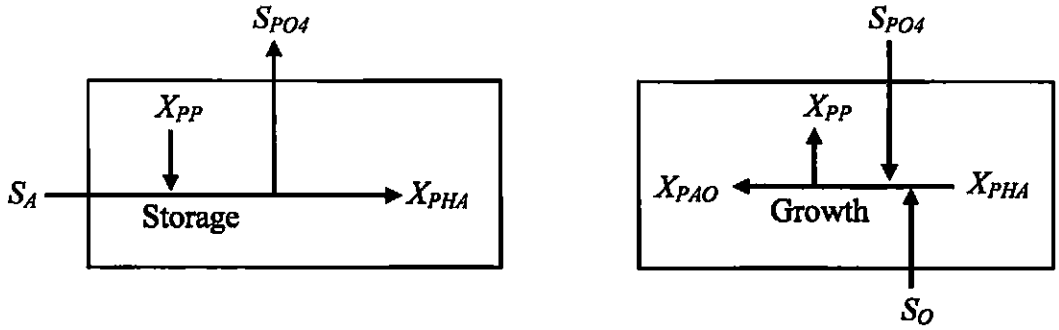

Fig. 6. Storage and growth processes involving PAO (modified from (Yang et al. 2006))

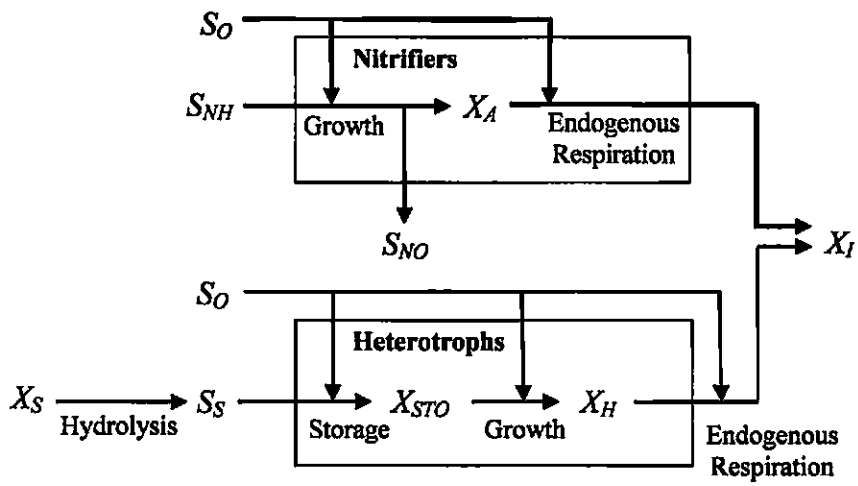

Fig. 7. Flow of substrate in ASM3 (modified from (Gujer et al. 1999))

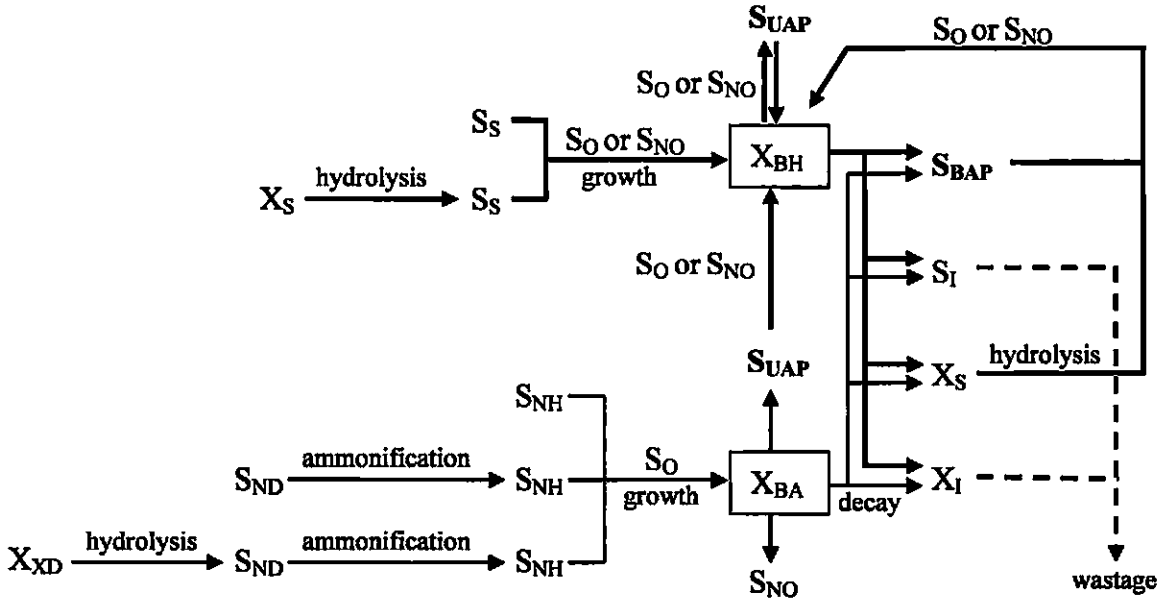

Fig. 8. Schematic description of the ASM1-SMP hybrid model (Lu et al. 2001)

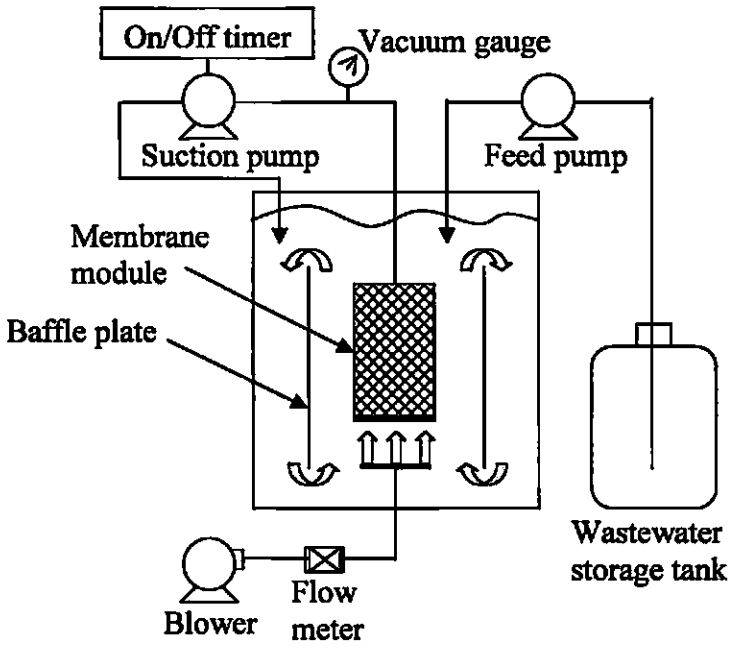

Fig. 9. Diagram of internal-loop-airlift reactor (Liu et al. 2003)

APPENDIX: MBR MODELS

ACTIVATED SLUDGE MODEL NO. 1

ASM1 stoichiometric coefficients

Component i		1	2	3	4	5	6	7	8
j	Process	S_I	S_S	X_I	X_S	$X_{B,H}$	$X_{B,A}$	X_P	S_O
1	Aerobic growth of heterotrophs		$-\frac{1}{Y_H}$			1			$-\frac{1-Y_H}{Y_H}$
2	Anoxic growth of heterotrophs		$-\frac{1}{Y_H}$			1			
3	Aerobic growth of autotrophs						1		$-\frac{4.57-Y_A}{Y_A}$
4	Decay of heterotrophs				$1-f_P$	−1		f_P	
5	Decay of autotrophs				$1-f_P$		−1	f_P	
6	Ammonification of soluble organic nitrogen								
7	Hydrolysis of entrapped organics		1		−1				
8	Hydrolysis of entrapped organic nitrogen								
Observed Conversion Rates		$r_i = \sum_j \nu_{ij}\rho_j$							
Stoichiometric parameters: Heterotrophic yield: Y_H Autotrophic yield: Y_A Fraction of biomass yielding particulates: f_P Mass N/Mass COD in biomass: i_{XB} Mass N/Mass COD in products from biomass: i_{XP}		Soluble inert organic matter [M(COD)L^{-3}]	Readily biodegradable substrate [M(COD)L^{-3}]	Particulate inert organic matter [M(COD)L^{-3}]	Slowly biodegradable substrate [M(COD)L^{-3}]	Active heterotrophic biomass [M(COD)L^{-3}]	Active autotrophic biomass [M(COD)L^{-3}]	Particulate products arising from biomass decay [M(COD)L^{-3}]	Oxygen (negative COD) [M(−COD)L^{-3}]

ASM1 stoichiometric coefficients (continued)

Component i / j	Process	9 S_{NO}	10 S_{NH}	11 S_{ND}	12 X_{ND}	13 S_{ALK}
1	Aerobic growth of heterotrophs		$-i_{XB}$			$-\frac{i_{XB}}{14}$
2	Anoxic growth of heterotrophs	$-\frac{1-Y_H}{2.86Y_H}$	$-i_{XB}$			$\frac{1-Y_H}{14\cdot 2.86Y_H}-\frac{i_{XB}}{14}$
3	Aerobic growth of autotrophs	$\frac{1}{Y_A}$	$-i_{XB}-\frac{1}{Y_A}$			$-\frac{i_{XB}}{14}-\frac{1}{7Y_A}$
4	Decay of heterotrophs				$i_{XB}-f_P i_{XP}$	
5	Decay of autotrophs				$i_{XB}-f_P i_{XP}$	
6	Ammonification of soluble organic nitrogen		1	−1		$\frac{1}{14}$
7	Hydrolysis of entrapped organics					
8	Hydrolysis of entrapped organic nitrogen			1	−1	
Observed Conversion Rates		$r_i=\sum_j \nu_{ij}\rho_j$				
Stoichiometric parameters: Heterotrophic yield: Y_H; Autotrophic yield: Y_A; Fraction of biomass yielding particulates: f_P; Mass *N*/Mass COD in biomass: i_{XB}; Mass *N*/Mass COD in products from biomass: i_{XP}		Nitrate and nitrite nitrogen [M(N)L^{-3}]	$NH_4^+ + NH_3$ nitrogen [M(N)L^{-3}]	Soluble biodegradable organic nitrogen [M(N)L^{-3}]	Particulate biodegradable organic nitrogen [M(N)L^{-3}]	Alkalinity – Molar units

ASM1 process kinetics

j	Process	Process rate expression, ρ_j [$ML^{-3}T^{-1}$]
1	Aerobic growth of heterotrophs	$\hat{\mu}_H \left(\frac{S_S}{K_S + S_S}\right)\left(\frac{S_O}{K_{O,H} + S_O}\right) X_{B,H}$
2	Anoxic growth of heterotrophs	$\hat{\mu}_H \left(\frac{S_S}{K_S + S_S}\right)\left(\frac{K_{O,H}}{K_{O,H} + S_O}\right)\left(\frac{S_{NO}}{K_{NO} + S_{NO}}\right) \eta_g X_{B,H}$
3	Aerobic growth of autotrophs	$\hat{\mu}_A \left(\frac{S_{NH}}{K_{NH} + S_{NH}}\right)\left(\frac{S_O}{K_{O,A} + S_O}\right) X_{B,A}$
4	Decay of heterotrophs	$b_H X_{B,H}$
5	Decay of autotrophs	$b_A X_{B,A}$
6	Ammonification of soluble organic nitrogen	$k_a S_{ND} X_{B,H}$
7	Hydrolysis of entrapped organics	$k_h \frac{X_S / X_{B,H}}{K_X + (X_S / X_{B,H})}\left[\left(\frac{S_O}{K_{O,H} + S_O}\right) + \eta_h \left(\frac{K_{O,H}}{K_{O,H} + S_O}\right)\left(\frac{S_{NO}}{K_{NO} + S_{NO}}\right)\right] X_{B,H}$
8	Hydrolysis of entrapped organic nitrogen	$\rho_7 (X_{ND} / X_S)$
Observed Conversion Rates		$r_i = \sum_j \nu_{ij} \rho_j$

Kinetic parameters:

Heterotrophic growth and decay:

$\hat{\mu}_H, K_S, K_{O,H}, K_{NO}, b_H$

Autotrophic growth and decay:

$\hat{\mu}_A, K_{NH}, K_{O,A}, b_A$

Correction factor for anoxic growth of heterotrophs: η_g

Ammonification: k_a

Hydrolysis: k_h, K_X

Correction factor for anoxic hydrolysis: η_h

ACTIVATED SLUDGE MODEL NO. 2

The continuity equation for all processes j and components c can be written as:

$$\sum_i \nu_{ji} \cdot i_{ci} = 0 \text{ over all components } i$$

where ν_{ji} = stoichiometric coefficient for component i in process j

i_{ci} = conversion factor to convert the units of component i to the units of material c

$$\text{e.g., } \nu_{1,PO_4} = -\left[\left(1-f_{S_I}\right)\cdot i_{PS_F} + f_{S_I}\cdot \nu_{1,ALK} - 1\cdot i_{PX_S}\right]/1$$

The reaction rate equation for component i can be computed from the sum:

$$r_i = \sum_j \nu_{ij}\rho_j \text{ overall processes } j$$

ASM2 component definition and units

i	Components		Units
1	S_{O_2}	Dissolved oxygen	g O_2 m^{-3}
2	S_F	Fermentable, readily biodegradable organic substrates	g COD m^{-3}
3	S_A	Fermentation products (acetate)	g COD m^{-3}
4	S_{NH_4}	Ammonium plus ammonia nitrogen (NH_4^+-N + NH_3-N)	g N m^{-3}
5	S_{NO_3}	Nitrate plus nitrite nitrogen (NO_3^- -N + NO_2^--N)	g N m^{-3}
6	S_{PO_4}	Inorganic soluble phosphorous, primarily ortho-phosphates	g P m^{-3}
7	S_I	Inert, soluble organic matter	g COD m^{-3}
8	S_{ALK}	Alkalinity of the wastewater	mol HCO_3 m^{-3}
9	S_{N_2}	Dinitrogen (N_2)	g N m^{-3}
10	X_I	Inert, particulate organic material	g COD m^{-3}
11	X_S	Slowly biodegradable substrates	g COD m^{-3}
12	X_H	Hetertrophic organisms	g COD m^{-3}
13	X_{PAO}	Phosphorous accumulating organisms (PAO)	g COD m^{-3}
14	X_{PP}	Poly-phosphate	g P m^{-3}
15	X_{PHA}	Cell internal storage product of PAOs	g COD m^{-3}
16	X_{AUT}	Nitrifying organisms	g COD m^{-3}
17	X_{TSS}	Total suspended solids (TSS)	g TSS m^{-3}
18	X_{MeOH}	Metal hydroxides	g TSS m^{-3}
19	X_{MeP}	Metal phosphate ($MePO_4$)	g TSS m^{-3}

ASM2 definition of parameters

Continuity conversion factors		Kinetic parameters (continued)	
i_{NS_I}	N content of inert soluble COD S_I	K_F	Saturation coefficient for growth on S_F
i_{NS_F}	N content of soluble substrate S_F	K_{fe}	Saturation coefficient for fermentation on S_F
i_{NX_I}	N content of inert particulate COD X_I	K_A	Saturation coefficient for S_A (acetate)
i_{NX_S}	N content of particulate substrate X_S	K_{NH_4}	Saturation coefficient for ammonium
i_{NBM}	N content in biomass X_H, X_{PAO}, X_{AUT}	K_P	Saturation coefficient for phosphorous
i_{PS_I}	P content of inert soluble COD S_I	K_{ALK}	Saturation coefficient for alkalinity
i_{PS_F}	P content of soluble substrate S_F	K_{PS}	Saturation coefficient for PP storage
i_{PX_I}	P content of inert particulate COD X_I	K_{PP}	Saturation coefficient for poly-phosphate
i_{PX_S}	P content of particulate substrate X_S	K_{MAX}	Maximum ratio for X_{PP}/X_{PAO}
i_{PBM}	P content in biomass X_H, X_{PAO}, X_{AUT}	K_{IPP}	Inhibition coefficient for X_{PP} storage
i_{TSSX_I}	TSS to X_I ratio	K_{PHA}	Saturation coefficient for PHA
i_{TSSX_S}	TSS to X_S ratio	k_{PRE}	Rate constant for P precipitation
i_{TSSBM}	TSS to biomass ratio for X_H, X_{PAO}, X_{AUT}	k_{RED}	Rate constant for redissolution
Stoichiometric constants		b_H	Rate constant for lysis of heterotrophs
f_{S_I}	Fraction of inert COD in particulate substrate	b_{PAO}	Rate constant for lysis of X_{PAO}
f_{X_I}	Fraction of inert COD generated in biomass lysis	b_{PP}	Rate constant for lysis of X_{PP}
Y_H	Yield coefficient	b_{PHA}	Rate constant for lysis of X_{PHA}
Y_{PAO}	Yield coefficient (biomass/PHA)	b_{AUT}	Rate constant for lysis of nitrifiers
Y_{PO_4}	PP requirement (S_{PO_4} release) for PHA storage	μ_H	Maximum growth rate of heterotrophs on substrate
Y_{PHA}	PHA requirement for PP storage	μ_{PAO}	Maximum growth rate of PAO
Y_{AUT}	Yield coefficient (bimass/nitrate)	μ_{AUT}	Maximum growth rate of nitrifiers
Kinetic parameters		η_{NO_3}	Anoxic hydrolysis or denitrification reduction factor
K_h	Hydrolysis rate constant	η_{fe}	Anaerobic hydrolysis reduction factor
K_{NO_3}	Saturation/inhibition coefficient for nitrate	q_{fe}	Maximum rate for fermentation
K_{O_2}	Saturation/inhibition coefficient for oxygen	q_{PHA}	Rate constant for storage of PHA
K_X	Saturation coefficient for particulate COD	q_{PP}	Rate constant for storage of PP

ASM2 stoichiometric coefficients

Component i		1	2	3	4	5	6
j	Process	S_{O2}	S_F	S_A	S_{NH4}	S_{NO3}	S_{PO4}
Hydrolysis processes:							
1	Aerobic		$1-f_{S_I}$		ν_{1,NH_4}		ν_{1,PO_4}
2	Anoxic		$1-f_{S_I}$		ν_{2,NH_4}		ν_{2,PO_4}
3	Anaerobic		$1-f_{S_I}$		ν_{3,NH_4}		ν_{3,PO_4}
Heterotrophic organisms: X_H							
4	Aerobic growth of X_H on S_F	$1-\frac{1}{Y_H}$	$-\frac{1}{Y_H}$				
5	Aerobic growth of X_H on S_A	$1-\frac{1}{Y_H}$		$-\frac{1}{Y_H}$			
6	Denitrification with S_F		$-\frac{1}{Y_H}$			$-\frac{1-Y_H}{2.86Y_H}$	
7	Denitrification with S_A			$-\frac{1}{Y_H}$		$-\frac{1-Y_H}{2.86Y_H}$	
8	Fermentation		-1	1			
9	Lysis of X_H						
Phosphorus accumulating organisms (PAO): X_{PAO}							
10	Storage of X_{PHA}			-1			Y_{PO_4}
11	Storage of X_{PP}	$-Y_{PHA}$					-1
12	Aerobic growth of X_{PAO}	$1-\frac{1}{Y_H}$					$-i_{PBM}$
13	Lysis of X_{PAO}						ν_{13,PO_4}
14	Lysis of X_{PP}						1
15	Lysis of X_{PHA}			1			
Nitrifying organisms (autotrophic organisms): X_{AUT}							
16	Aerobic growth of X_{AUT}	$-\frac{4.57-Y_A}{Y_A}$			$-i_{NBM}-\frac{1}{Y_A}$	$\frac{1}{Y_A}$	$-i_{PBM}$
17	Lysis of X_{AUT}				ν_{17,NH_4}		ν_{17,PO_4}
Simultaneous precipitation of phosphorus with ferric hydroxide $Fe(OH)_3$							
18	Precipitation						-1
19	Redissolution						1

ASM2 stoichiometric coefficients (continued)

Component i		7	8	9	10	11	12	13
j	Process	S_I	S_{ALK}	S_{N2}	X_I	X_S	X_H	X_{PAO}
Hydrolysis processes:								
1	Aerobic	f_{S_I}	$\nu_{1,ALK}$			-1		
2	Anoxic	f_{S_I}	$\nu_{2,ALK}$			-1		
3	Anaerobic	f_{S_I}	$\nu_{3,ALK}$			-1		
Heterotrophic organisms: X_H								
4	Aerobic growth of X_H on S_F						1	
5	Aerobic growth of X_H on S_A						1	
6	Denitrification with S_F			$\frac{1-Y_H}{2.86Y_H}$			1	
7	Denitrification with S_A			$\frac{1-Y_H}{2.86Y_H}$			1	
8	Fermentation							
9	Lysis of X_H				f_{X_I}	$1-f_{X_I}$	-1	
Phosphorus accumulating organisms (PAO): X_{PAO}								
10	Storage of X_{PHA}							
11	Storage of X_{PP}							
12	Aerobic growth of X_{PAO}							1
13	Lysis of X_{PAO}				f_{X_I}	$1-f_{X_I}$		-1
14	Lysis of X_{PP}							
15	Lysis of X_{PHA}							
Nitrifying organisms (autotrophic organisms): X_{AUT}								
16	Growth of X_{AUT}							
17	Lysis of X_{AUT}				f_{X_I}	$1-f_{X_I}$		
Simultaneous precipitation of phosphorus with ferric hydroxide $Fe(OH)_3$								
18	Precipitation		$\nu_{19,ALK}$					
19	Redissolution		$\nu_{20,ALK}$					

ASM2 conversion factors

$c\downarrow$	$i\rightarrow$	S_{O2}	S_F	S_A	S_{NH4}	S_{NO3}	S_{PO4}	S_I	S_{ALK}	S_{N2}
1	g COD	-1	1	1		$-64/14$		1		$-24/14$
2	g N		i_{NS_F}		1	1		i_{NS_I}		1
3	g P		i_{PS_F}				1	i_{PS_I}		
4	mole$^+$			$-1/64$	$+1/14$	$-1/14$	$-1.5/31$		-1	

ASM2 stoichiometric coefficients (continued)

Component i		14	15	16	17	18	19
j	Process	X_{PP}	X_{PHA}	X_{AUT}	X_{TSS}	X_{MeOH}	X_{MeP}
Hydrolysis processes:							
1	Aerobic				$\nu_{1,TSS}$		
2	Anoxic				$\nu_{2,TSS}$		
3	Anaerobic				$\nu_{3,TSS}$		
Heterotrophic organisms: X_H							
4	Aerobic growth of X_H on S_F						
5	Aerobic growth of X_H on S_A						
6	Denitrification with S_F						
7	Denitrification with S_A						
8	Fermentation						
9	Lysis of X_H						
Phosphorus accumulating organisms (PAO): X_{PAO}							
10	Storage of X_{PHA}	$-Y_{PO_4}$	1				
11	Storage of X_{PP}	1	$-Y_{PHA}$				
12	Aerobic growth of X_{PAO}		$-\frac{1}{Y_H}$				
13	Lysis of X_{PAO}						
14	Lysis of X_{PP}	−1					
15	Lysis of X_{PHA}		−1				
Nitrifying organisms (autotrophic organisms): X_{AUT}							
16	Growth of X_{AUT}			1			
17	Lysis of X_{AUT}			−1			
Simultaneous precipitation of phosphorus with ferric hydroxide $Fe(OH)_3$							
18	Precipitation				1.42	−3.45	4.87
19	Redissolution				−1.42	3.45	−4.87

ASM2 conversion factors (continued)

$c\downarrow$	$i\rightarrow$	X_I	X_S	X_H	X_{PAO}	X_{PP}	X_{PHA}	X_{AUT}	X_{TSS}	X_{MeOH}	X_{MeP}
1	g COD	1	1	1	1		1	1			
2	g N	i_{NX_I}	i_{NX_S}	i_{NBM}	i_{NBM}			i_{NBM}			
3	g P	i_{PX_I}	i_{PX_S}	i_{PBM}	i_{PBM}	1		i_{PBM}			0.205
5	g TSS	i_{TSSX_I}	i_{TSSX_S}	i_{TSSBM}	i_{TSSBM}	3.23	0.60	i_{TSSBM}	−1	1	1

ASM2 process kinetics

Process		Process rate expression, ρ_j [$ML^{-3}T^{-1}$]
Hydrolysis process:		
1	Aerobic hydrolysis	$K_h \cdot \frac{S_{O_2}}{K_{O_2}+S_{O_2}} \cdot \frac{X_S/X_H}{K_X+X_S/X_H} \cdot X_H$
2	Anoxic hydrolysis	$K_h \cdot \eta_{NO_3} \cdot \frac{K_{O_2}}{K_{O_2}+S_{O_2}} \cdot \frac{S_{NO_3}}{K_{NO_3}+S_{NO_3}} \cdot \frac{X_S/X_H}{K_X+X_S/X_H} \cdot X_H$
3	Anaerobic hydrolysis	$K_h \cdot \eta_{fe} \cdot \frac{K_{O_2}}{K_{O_2}+S_{O_2}} \cdot \frac{K_{NO_3}}{K_{NO_3}+S_{NO_3}} \cdot \frac{X_S/X_H}{K_X+X_S/X_H} \cdot X_H$
Heterotrophic organisms: X_H		
4	Growth of X_H on fermentable substrates, S_F	$\mu_H \cdot \frac{S_{O_2}}{K_{O_2}+S_{O_2}} \cdot \frac{S_F}{K_F+S_F} \cdot \frac{S_F}{S_F+S_A} \cdot \frac{S_{NH_4}}{K_{NH_4}+S_{NH_4}} \cdot \frac{S_{PO_4}}{K_P+S_{PO_4}} \cdot \frac{S_{ALK}}{K_{ALK}+S_{ALK}} \cdot X_H$
5	Growth of X_H on fermentable products, S_A	$\mu_H \cdot \frac{S_{O_2}}{K_{O_2}+S_{O_2}} \cdot \frac{S_A}{K_A+S_A} \cdot \frac{S_A}{S_F+S_A} \cdot \frac{S_{NH_4}}{K_{NH_4}+S_{NH_4}} \cdot \frac{S_{PO_4}}{K_P+S_{PO_4}} \cdot \frac{S_{ALK}}{K_{ALK}+S_{ALK}} \cdot X_H$
6	Denitrification on fermentable substrates, S_F	$\mu_H \cdot \eta_{NO_3} \cdot \frac{K_{O_2}}{K_{O_2}+S_{O_2}} \cdot \frac{S_F}{K_F+S_F} \cdot \frac{S_F}{S_F+S_A} \cdot \frac{S_{NH_4}}{K_{NH_4}+S_{NH_4}} \cdot \frac{S_{NO_3}}{K_{NO_3}+S_{NO_3}} \cdot \frac{S_{ALK}}{K_{ALK}+S_{ALK}} \cdot \frac{S_{PO_4}}{K_P+S_{PO_4}} \cdot X_H$
7	Denitrification on fermentable products, S_A	$\mu_H \cdot \eta_{NO_3} \cdot \frac{K_{O_2}}{K_{O_2}+S_{O_2}} \cdot \frac{S_A}{K_A+S_A} \cdot \frac{S_A}{S_F+S_A} \cdot \frac{S_{NH_4}}{K_{NH_4}+S_{NH_4}} \cdot \frac{S_{NO_3}}{K_{NO_3}+S_{NO_3}} \cdot \frac{S_{ALK}}{K_{ALK}+S_{ALK}} \cdot \frac{S_{PO_4}}{K_P+S_{PO_4}} \cdot X_H$
8	Fermentation	$q_{fe} \cdot \frac{K_{O_2}}{K_{O_2}+S_{O_2}} \cdot \frac{K_{NO_3}}{K_{NO_3}+S_{NO_3}} \cdot \frac{S_F}{K_{fe}+S_F} \cdot \frac{S_{ALK}}{K_{ALK}+S_{ALK}} \cdot X_H$
9	Lysis of X_H	$b_H \cdot X_H$

ASM2 process kinetics (continued)

Process		Process rate expression, ρ_j [$ML^{-3}T^{-1}$]
Phosphorous-accumulating organisms (PAO): X_{PAO}		
10	Storage of X_{PHA}	$q_{PHA} \cdot \frac{S_A}{K_A + S_A} \cdot \frac{S_{ALK}}{K_{ALK} + S_{ALK}} \cdot \frac{X_{PP}/X_{PAO}}{K_{PP} + X_{PP}/X_{PAO}} \cdot X_{PAO}$
11	Storage of X_{PP}	$q_{PP} \cdot \frac{S_{O_2}}{K_{O_2} + S_{O_2}} \cdot \frac{S_{PO_4}}{K_{PS} + S_{PO_4}} \cdot \frac{S_{ALK}}{K_{ALK} + S_{ALK}} \cdot \frac{X_{PHA}/X_{PAO}}{K_{PHA} + X_{PHA}/X_{PAO}} \cdot \frac{K_{MAX} - X_{PP}/X_{PAO}}{K_{IPP} + K_{MAX} - X_{PP}/X_{PAO}} \cdot X_{PAO}$
12	Aerobic growth on X_{PHA}	$\mu_{PAO} \cdot \frac{S_{O_2}}{K_{O_2} + S_{O_2}} \cdot \frac{S_{NH_4}}{K_{NH_4} + S_{NH_4}} \cdot \frac{S_{ALK}}{K_{ALK} + S_{ALK}} \cdot \frac{S_{PO_4}}{K_P + S_{PO_4}} \cdot \frac{X_{PHA}/X_{PAO}}{K_{PHA} + X_{PHA}/X_{PAO}} \cdot X_{PAO}$
13	Lysis of X_{PAO}	$b_{PAO} \cdot X_{PAO} \cdot S_{ALK} / (K_{ALK} + S_{ALK})$
14	Lysis of X_{PP}	$b_{PP} \cdot X_{PP} \cdot S_{ALK} / (K_{ALK} + S_{ALK})$
15	Lysis of X_{PHA}	$b_{PHA} \cdot X_{PHA} \cdot S_{ALK} / (K_{ALK} + S_{ALK})$
Nitrifying organisms (autotrophic organisms): X_{AUT}		
16	Growth of X_{AUT}	$\mu_{AUT} \cdot \frac{S_{O_2}}{K_{O_2} + S_{O_2}} \cdot \frac{S_{NH_4}}{K_{NH_4} + S_{NH_4}} \cdot \frac{S_{PO_4}}{K_P + S_{PO_4}} \cdot \frac{S_{ALK}}{K_{ALK} + S_{ALK}} \cdot X_{AUT}$
17	Lysis of X_{AUT}	$b_{AUT} \cdot X_{AUT}$
Simultaneous precipitation of phosphorus with ferric hydroxide $Fe(OH)_3$		
18	Precipitation	$k_{PRE} \cdot S_{PO4} \cdot X_{MeOH}$
19	Redissolution	$k_{RED} \cdot X_{MeP} \cdot S_{ALK} / (K_{ALK} + S_{ALK})$

ACTIVATED SLUDGE MODEL NO. 2d

Additions and changes to ASM2:

Stoichiometric coefficients

	Process	S_{O2}	S_{N2}	S_{NO3}	S_{PO4}	X_{PAO}	X_{PP}	X_{PHA}
Phosphorus accumulating organisms (PAO): X_{PAO}								
11	Aerobic storage of X_{PP}	$-Y_{PHA}$			-1		1	$-Y_{PHA}$
12	Anoxic storage of X_{PP}		$-\nu_{12,NO_3}$	ν_{12,NO_3}	-1		1	$-Y_{PHA}$
13	Aerobic growth of X_{POA}	ν_{13,O_2}			$-i_{PBM}$	1		$-\frac{1}{Y_H}$
14	Anoxic growth of X_{POA}		$-\nu_{14,NO_3}$	ν_{14,NO_3}	$-i_{PBM}$	1		$-\frac{1}{Y_H}$

ASM2 conversion factors

c ↓	i →	X_I	X_S	X_H	X_{PAO}	X_{PP}	X_{PHA}	X_{AUT}	X_{TSS}	X_{MeOH}	X_{MeP}
4	mole$^+$					$-1/31^*$					

*only change from ASM2 conversion factor matrix; ASM2 does not account for K^+ and Mg^{2+} so this factor must compensate for their charge

Process kinetics

	Process	Process rate expression, ρ_j [$ML^{-3}T^{-1}$]
Phosphorous-accumulating organisms (PAO): X_{PAO}		
12	Anoxic storage of X_{PP}	$q_{PP}\cdot\eta_{NO_3}\cdot\frac{K_{O_2}}{S_{O_2}}\cdot\frac{S_{NO_3}}{K_{NO_3}+S_{NO_3}}\cdot\frac{S_{O_2}}{K_{O_2}+S_{O_2}}\cdot\frac{S_{PO_4}}{K_{PS}+S_{PO_4}}\cdot\frac{S_{ALK}}{K_{ALK}+S_{ALK}}\cdot\frac{X_{PHA}/X_{PAO}}{K_{PHA}+X_{PHA}/X_{PAO}}\cdot\frac{K_{MAX}-X_{PP}/X_{PAO}}{K_{PP}+K_{MAX}-X_{PP}/X_{PAO}}\cdot X_{PAO}$
14	Anoxic growth on X_{PP}	$\mu_{PAO}\cdot\eta_{NO_3}\cdot\frac{K_{O_2}}{S_{O_2}}\cdot\frac{S_{NO_3}}{K_{NO_3}+S_{NO_3}}\cdot\frac{S_{O_2}}{K_{O_2}+S_{O_2}}\cdot\frac{S_{PO_4}}{K_P+S_{PO_4}}\cdot\frac{S_{NH_4}}{K_{NH_4}+S_{NH_4}}\cdot\frac{S_{ALK}}{K_{ALK}+S_{ALK}}\cdot\frac{X_{PHA}/X_{PAO}}{K_{PHA}+X_{PHA}/X_{PAO}}\cdot X_{PAO}$

ACTIVATED SLUDGE MODEL NO. 3

The following equations can be used to obtain all values of x_j, y_j, and z_j in the stoichiometric matrix from the composition matrix:

$$\sum_i \nu_{j,i} \cdot i_{k,i} = 0 \text{ for } i = 1 \text{ to } 12$$

$$\nu_{j,13} = \sum_i \nu_{j,i} \cdot i_{4,i} = 0 \text{ for } i = 8 \text{ to } 12$$

The reaction rate equation for component i can be computed from the sum:

$$r_i = \sum_j \nu_{ij} \rho_j \text{ overall processes } j$$

ASM2 component definition and units

i	Components		Units
1	S_{O_2}	Dissolved oxygen	g O_2 m^{-3}
2	S_I	Inert soluble organic material	g COD m^{-3}
3	S_S	Readily biodegradable organic substrates	g COD m^{-3}
4	S_{NH_4}	Ammonium plus ammonia nitrogen (NH_4^+-N + NH_3-N)	g N m^{-3}
5	S_{N_2}	Dinitrogen (N_2)	g N m^{-3}
6	S_{NOX}	Nitrate plus nitrite nitrogen (NO_3^--N + NO_2^--N)	g N m^{-3}
7	S_{ALK}	Alkalinity of the wastewater	mol HCO_3 m^{-3}
8	X_I	Inert particulate organic material	g COD m^{-3}
9	X_S	Slowly biodegradable substrates	g COD m^{-3}
10	X_H	Hetertrophic organisms	g COD m^{-3}
11	X_{STO}	Cell internal storage product of heterotrophic organisms	g COD m^{-3}
12	X_A	Nitrifying organisms	g COD m^{-3}
13	X_{TSS}	Suspended solids (SS)	g SS m^{-3}

ASM3 definition of parameters

Composition parameters		**Kinetic parameters**	
i_{N,S_I}	N content of S_I	k_H	Hydrolysis rate constant
i_{N,S_S}	N content of S_S	k_{STO}	Storage rate constant
i_{N,X_I}	N content of X_I	K_X	Hydrolysis saturation constant
i_{N,X_S}	N content of X_S	K_{O_2}	Saturation constant for S_{NO_2}
i_{NBM}	N content in biomass X_H, X_A	K_{NOX}	Saturation constant for S_{NOX}
i_{SS,X_I}	SS to COD ratio for X_I	K_S	Saturation constant for substrate S_s
i_{SS,X_S}	SS to COD ratio for X_S	K_{STO}	Saturation constant for X_{STO}
$i_{SS,BM}$	SS to COD ratio for biomass, X_H, X_A	K_{NH_4}	Saturation constant for ammonium, S_{NH_4}
		K_{ALK}	Saturation constant for alkalinity for X_H
Stoichiometric constants		K_{A,NH_4}	Ammonium substrate saturation for X_A
f_{S_I}	Production of S_I in hydrolysis	K_{A,O_2}	Oxygen saturation for nitrifiers
f_{X_I}	Production of X_I in endogenous respiration	$K_{A,ALK}$	Bicarbonate saturation for nitrifiers
Y_{H,O_2}	Aerobic yield of heterotrophic biomass	η_{NOX}	Anoxic reduction factor
$Y_{H,NOX}$	Anoxic yield of heterotrophic biomass	μ_H	Herterotrophic max growth rate
Y_{STO,O_2}	Aerobic yield of stored product per S_S	μ_A	Autotrophic max growth rate
$Y_{STO,NOX}$	Anoxic yield of stored product per S_S	b_{H,O_2}	Aerobic endogenous respiration rate of X_H
Y_A	Yield of autrophic biomass per NO_3^--N	$b_{H,NOX}$	Anoxic endogenous respiration rate of X_H
		b_{STO,O_2}	Aerobic endogenous respiration rate of X_{STO}
		$b_{STO,NOX}$	Anoxic endogenous respiration rate of X_{STO}
		b_{A,O_2}	Aerobic endogenous respiration rate of X_A
		$b_{A,NOX}$	Anoxic endogenous respiration rate of X_A

ASM3 stoichiometric coefficients and composition matrix

Component i		1	2	3	4	5	6	7
j	Process	S_{O2}	S_I	S_S	S_{NH4}	S_{N2}	S_{NOX}	S_{ALK}
1	Hydrolysis		f_{S_I}	x_1	y_1			z_1
Heterotrophic organisms, aerobic and denitrifying activity								
2	Aerobic storage of S_S	x_2		-1	y_2			z_2
3	Anoxic storage of S_S			-1	y_3	$-x_3$	x_3	z_3
4	Aerobic growth of X_H	x_4			y_4			z_4
5	Anoxic growth of X_H				y_5	$-x_5$	x_5	z_5
6	Aerobic endogenous respiration of X_H	x_6			y_6			z_6
7	Anoxic endogenous respiration of X_H				y_7	$-x_7$	x_7	z_7
8	Aerobic endogenous respiration of X_{STO}	x_8						z_8
9	Anoxic endogenous respiration of X_{STO}					$-x_9$	x_9	z_9
Autotrophic organisms, nitrifying activity								
10	Aerobic growth of X_A	x_{10}			y_{10}		$1/Y_A$	z_{10}
11	Aerobic endogenous respiration of X_A	x_{11}			y_{11}			z_{11}
12	Anoxic endogenous respiration of X_A				y_{12}	$-x_{12}$	x_{12}	z_{12}
Composition matrix, $i_{k,i}$								
k	*Conservatives*							
1	ThOD [g ThOD]	-1	1	1		-1.71	-4.57	
2	Nitrogen [g N]		i_{N,S_I}	i_{N,S_S}	1	1	1	
3	Ionic Charge [Mole +]				1/14		$-1/14$	-1
	Observables							
4	SS [g SS]							

ASM3 stoichiometric coefficients and composition matrix (continued)

Component i		8	9	10	11	12	13
j	Process	X_I	X_S	X_H	X_{STO}	X_A	X_{SS}
1	Hydrolysis		-1				$-i_{X_S}$
Heterotrophic organisms, aerobic and denitrifying activity							
2	Aerobic storage of S_S				Y_{STO,O_2}		t_2
3	Anoxic storage of S_S				$Y_{STO,NOX}$		t_3
4	Aerobic growth of X_H			1	$-1/Y_{H,O_2}$		t_4
5	Anoxic growth of X_H			1	$-1/Y_{H,NOX}$		t_5
6	Aerobic endogenous respiration X_H	f_I		-1			t_6
7	Anoxic endogenous respiration of X_H	f_I		-1			t_7
8	Aerobic endogenous respiration X_{STO}				-1		t_8
9	Anoxic endogenous respiration of X_{STO}				-1		t_9
Autotrophic organisms, nitrifying activity							
10	Aerobic growth of X_A					1	t_{10}
11	Aerobic endogenous respiration X_A	f_I				-1	t_{11}
12	Anoxic endogenous respiration of X_A	f_I				-1	t_{12}
Composition matrix, $i_{k,i}$							
k	*Conservatives*						
1	ThOD	1	1	1	1	1	
2	Nitrogen	i_{N,X_I}	i_{N,X_I}	$i_{N,BM}$		$i_{N,BM}$	
3	Ionic Charge						
	Observables						
4	SS	i_{SS,X_I}	i_{SS,X_S}	$i_{SS,BM}$	0.60	$i_{SS,BM}$	

ASM3 process kinetics

Component i		Process rate expression, ρ_j [$ML^{-3}T^{-1}$]
j	Process	
1	Hydrolysis	$k_H \frac{X_S/X_H}{K_X+(X_S/X_H)} X_H$
Heterotrophic organisms, aerobic and denitrifying activity		
2	Aerobic storage of S_S	$k_{STO} \cdot \frac{S_{O_2}}{K_{O_2}+S_{O_2}} \cdot \frac{S_S}{K_S+S_S} \cdot X_H$
3	Anoxic storage of S_S	$k_{STO} \cdot \eta_{NOX} \cdot \frac{K_{O_2}}{K_{O_2}+S_{O_2}} \cdot \frac{S_{NOX}}{K_{NOX}+S_{NOX}} \cdot \frac{S_S}{K_S+S_S} \cdot X_H$
4	Aerobic growth of X_H	$\mu_H \cdot \frac{S_{O_2}}{K_{O_2}+S_{O_2}} \cdot \frac{S_{NH_4}}{K_{NH_4}+S_{NH_4}} \cdot \frac{S_{ALK}}{K_{ALK}+S_{ALK}} \cdot \frac{X_{STO}/X_H}{K_{STO}+X_{STO}/X_H} \cdot X_H$
5	Anoxic growth of X_H	$\mu_H \cdot \eta_{NOX} \cdot \frac{K_{O_2}}{K_{O_2}+S_{O_2}} \cdot \frac{S_{NOX}}{K_{NOX}+S_{NOX}} \cdot \frac{S_{NH_4}}{K_{NH_4}+S_{NH_4}} \cdot \frac{S_{ALK}}{K_{ALK}+S_{ALK}} \cdot \frac{X_{STO}/X_H}{K_{STO}+X_{STO}/X_H} \cdot X_H$
6	Aerobic endogenous respiration of X_H	$b_{H,O_2} \cdot \frac{S_{O_2}}{K_{O_2}+S_{O_2}} \cdot X_H$
7	Anoxic endogenous respiration of X_H	$b_{H,NOX} \cdot \frac{K_{O_2}}{K_{O_2}+S_{O_2}} \cdot \frac{S_{NOX}}{K_{NOX}+S_{NOX}} \cdot X_H$
8	Aerobic endogenous respiration of X_{STO}	$b_{STO,O_2} \cdot \frac{S_{O_2}}{K_{O_2}+S_{O_2}} \cdot X_{STO}$
9	Anoxic endogenous respiration of X_{STO}	$b_{STO,NOX} \cdot \frac{K_{O_2}}{K_{O_2}+S_{O_2}} \cdot \frac{S_{NOX}}{K_{NOX}+S_{NOX}} \cdot X_{STO}$
Autotrophic organisms, nitrifying activity		
10	Aerobic growth of X_A	$\mu_A \cdot \frac{S_{O_2}}{K_{A,O_2}+S_{O_2}} \cdot \frac{S_{NH_4}}{K_{A,NH_4}+S_{NH_4}} \cdot \frac{S_{ALK}}{K_{A,ALK}+S_{ALK}} \cdot X_A$
11	Aerobic endogenous respiration of X_A	$b_{A,O_2} \cdot \frac{S_{O_2}}{K_{A,O_2}+S_{O_2}} \cdot X_A$
12	Anoxic endogenous respiration of X_A	$b_{A,NOX} \cdot \frac{K_{A,O_2}}{K_{A,O_2}+S_{O_2}} \cdot \frac{S_{NOX}}{K_{A,NOX}+S_{NOX}} \cdot X_A$

SOLUBLE MICROBIAL PRODUCTS MODEL

Furumai-Rittmann model (1992)

Biomass
1. Heterotrophs (X_h): $V\frac{dX_h}{dt} = Q^0X_h^0 - Q^eX_h^e - Q^wX_h^w + \left(Y_hR_hX_h + Y_PR_3X_h - b_hX_h - (1/\gamma_s)R_{2h}X_h\right)V$
2. Nitrifiers ($X_n = X_{ns}$ or X_{nb}): $V\frac{dX_n}{dt} = Q^0X_n^0 - Q^eX_n^e - Q^wX_n^w + \left(Y_nR_nX_n - b_nX_n - (1/\gamma_s)R_{2n}X_h\right)V$
3. Inert Biomass (X_i): $V\frac{dX_i}{dt} = Q^0X_i^0 - Q^eX_i^e - Q^wX_i^w + (1-f_d)\sum b_jX_jV$ (j = h, ns, nb)

Substrate and products
1. Substrate COD (S): $V\frac{dS}{dt} = Q^0\left(S^0 - S\right) - M_hX_hV$
2. $NH_4^+ - N$ ($N1$): $V\frac{dN1}{dt} = Q^0\left(N1^0 - N1\right) - \left(\begin{array}{l} M_{ns}X_{ns} + \gamma_nY_hM_hX_h + \gamma_nY_PR_{3h}X_h - \gamma_nf_d\sum b_jX_j \\ -\gamma_nR_3X_h\left[\frac{\sum k_{2j}X_j}{\sum\left(k_{1j}M_jX_j + \sum k_{2j}X_j\right)}\right] \end{array}\right)V$ (j = h, ns, nb)
3. $NO_2^- - N$ ($N2$ N2): $V\frac{dN2}{dt} = Q^0\left(N2^0 - N2\right) - \left(M_{nb}X_{nb} - (1-\gamma_nY_{ns})M_{ns}X_{ns}\right)V$
4. $NO_3^- - N$ (N2): $V\frac{dN3}{dt} = Q^0\left(N3^0 - N3\right) + (1-\gamma_nY_{nb})M_{nb}X_{nb}V$

Substrate and products
5. O_2 (O): $V\frac{dO}{dt}=Q^0\left(O^0-O\right)+\begin{pmatrix}K_{La}\left(O_S-O\right)-\left(1-\gamma_s Y_h\right)\beta_h M_h X_h-\left(1-\gamma_s Y_P\right)\beta_h R_3 X_h+\beta_h R_{1h} X_h \\ -\sum\left(1-\gamma_n Y_j\right)\beta_j M_j X_j+\sum\beta_j R_{1j} X_j-f_d\gamma_s\left(b_h X_h+\sum b_j X_j\right)\end{pmatrix}V$ (j = ns and nb)
6. Soluble Microbial Products (P): $V\frac{dP}{dt}=-Q^0P+\left(\sum\left(R_{1j}+R_{2j}\right)X_j-R_3X_h\right)V$ (j = h, ns, nb)
7. Total of originally formed SMP (P^0): $V\frac{dP^0}{dt}=-Q^0P^0+\sum\left(R_{1j}+R_{2j}\right)X_jV$ (j = h, ns, nb)
M: Specific substrate consumption rate $=q_m\left[\text{Sub}\right]\frac{\left[O_2\right]/\left(K_s+\left[\text{Sub}\right]\right)}{K_o+\left[O_2\right]}$ ([Sub] = S, N1, or N2)
R1: Specific UAP formation rate $=k_1M$
R2: Specific BAP formation rate $=k_2$
R3: Specific SMP consumption rate $=k_{3m}\left(P/P^0\right)$

Notations	
b	Decay rate constant [day-1]
b'	Overall decay rate constant $=b+\left(1/\gamma_S\right)k_2$ [day^{-1}]
COD	COD concentration = COD_S+COD_P [mgCOD/L]
COD_P	Code concentration of SMP [mgCOD/L]
COD_S	COD concentration of organic substrate [mgCOD/L]
f_d	Biodegradable fraction of active biomass [-]
k_1	UAP formation rate constant [$mgCOD_P\ mgCOD_S^{-1}$]
k_2	BAP formation rate constant [$mgCOD_P\ mgCOD_{cell}^{-1}\ day^{-1}$]
k_{3m}	Multiple substrate degradation rate constant [$mgCOD_P\ mgCOD_{cell}^{-1}\ day^{-1}$]
K_S	Saturation constant for substrate (electron donor) [mg/L]
K_O	Saturation constant for oxygen (electron acceptor) [mgO_2/L]
K_{La}	Overall oxygen transfer coefficient [day^{-1}]
O	Dissolved oxygen [mgO_2/L]
O_S	Saturation concentration of oxygen [mgO_2/L]

Notations	
P	SMP concentration [$mgCOD_P/L$]
P^0	Originally formed SMP concentration [$mgCOD_P/L$]
q_m	Maximum specific substrate consumption rate [$mgCOD_P\ mgCOD_{cell}^{-1}\ day^{-1}$]
Q	Flow rate [$L\ day^{-1}$]
S	Substrate concentration [mg/L]
SON	Soluble organic nitrogen [mgN/L]
V	Reactor volume [L]
X	Biomass concentration [mgCOD/L]
Y	Growth yield [$mgCOD_{cell}\ mg^{-1}$]
Y_P	Growth yield associated with SMP degradation [$mgCOD_{cell}\ mgCOD_P^{-1}$]
B	Oxygen demand for substrate consumption [$mgCOD\ mg^{-1}$]
γ_s	Conversion coefficient of biomass concentrations to COD [$mgCOD_{cell}\ mgCOD^{-1}$]
γ_n	Nitrogen content in biomass [$mgN\ mgCOD_{cell}^{-1}$]

Subscript	
h	Heterotrophs or heterotrophic oxidation
n	Nitrifiers
ns	NH_4 oxidizers or NH_4 oxidation
nb	NO_2 oxidizers of NO_2 oxidation
e	Steady-state condition

Superscript	
0	Influent flow, except for P
e	Effluent flow
w	Wasted flow

ASM1-SMP HYBRID MODEL

ASM1-SMP hybrid stoichiometric coefficients

Component i		1	2	3	4	5	6	7a	7a
j	Process	S_I	S_S	X_I	X_S	$X_{B,H}$	$X_{B,A}$	X_{UAP}	X_{BAP}
1	Aerobic growth of heterotrophs		$-\frac{1}{Y_H}$			1		$\gamma_{UAP,H}$	
	Aerobic growth of heterotrophs from SMP					1		$\gamma_{UAP,H}$	$-\frac{1}{Y_{SMP}}$
2	Anoxic growth of heterotrophs		$-\frac{1}{Y_H}$			1		$\gamma_{UAP,H}$	
	Anoxic growth of heterotrophs from SMP					1		$\gamma_{UAP,H}$	$-\frac{1}{Y_{SMP}}$
3	Aerobic growth of autotrophs						1	$\gamma_{UAP,A}$	
4	Decay of heterotrophs			f_P	$1-f_P$	-1			
5	BAP formation from decay of heterotrophs	f_B				-1			$1-f_B$
6	Decay of autotrophs			f_P	$1-f_P$		-1		$1-f_B$
7	BAP formation from decay of autotrophs	f_B					-1		
8	Ammonification of soluble organic nitrogen								
9	Hydrolysis of entrapped organics				-1				1
10	Hydrolysis of entrapped organic nitrogen								

Components:

S_{BAP} = Biomass-associated product, g COD m^{-3}

S_{UAP} = Utilization-associated product, g COD m^{-3}

S_{SMP} = Total soluble microbial products, equal to S_{BAP} plus S_{UAP}, g COD m^{-3}

Stoichiometric Parameters:

Y_{SMP} = Heterotrophic yield coefficient from SMP, g COD g COD^{-1}

f_B = Inert fraction of biomass leading to soluble products, dimensionless

i_{XB} = Mass N/mass COD in biomass, g N g COD^{-1}

ASM1-SMP hybrid stoichiometric coefficients (continued)

Component i		8	9	10	11	12
j	Process	S_O	S_{NO}	S_{NH}	S_{ND}	X_{ND}
1	Aerobic growth of heterotrophs	$-\frac{1-Y_H}{Y_H}$		$-i_{XB}$		
	Aerobic growth of heterotrophs from SMP	$-\frac{1-Y_{SMP}}{Y_{SMP}}$		$-i_{XB}$		
2	Anoxic growth of heterotrophs		$-\frac{1-Y_H}{2.86Y_H}$	$-i_{XB}$		
	Anoxic growth of heterotrophs from SMP		$-\frac{1-Y_{SMP}}{2.86Y_{SMP}}$	$-i_{XB}$		
3	Aerobic growth of autotrophs	$-\frac{4.57-Y_A}{Y_A}$	$\frac{1}{Y_A}$	$-i_{XB}-\frac{1}{Y_A}$		
4	Decay of heterotrophs					$i_{XB}-f_P i_{XP}$
5	BAP formation from decay of heterotrophs				$i_{XB}-f_B i_{XP}$	
6	Decay of autotrophs					$i_{XB}-f_P i_{XP}$
7	BAP formation from decay of autotrophs				$i_{XB}-f_B i_{XP}$	
8	Ammonification of soluble organic nitrogen			1	–1	
9	Hydrolysis of entrapped organics					
10	Hydrolysis of entrapped organic nitrogen				1	–1

Kinetic Parameters:

$b_{BAP,A}$ = Autotrophic decay coefficient for formation of BAP, day^{-1}

$b_{BAP,H}$ = Heterotrophic decay coefficient for formation of BAP, day^{-1}

K_{SMP} = SMP half-saturation coefficient for heterotrophic biomass, g COD m^{-3}

μ_{SMP} = Maximum specific growth rate of SMP for heterotrophs, day^{-1}

$\gamma_{UAP,H}$ = UAP formation constant of autotrophs, dimensionless

$\gamma_{UAP,A}$ = UAP formation constant of heterotrophs, dimensionless

ASM1-SMP hybrid process kinetics

j	Process	Process rate expression, ρ_j [$ML^{-3}T^{-1}$]
1	Aerobic growth of heterotrophs	$\mu_H\left(\frac{S_S}{K_S+S_S}\right)\left(\frac{S_O}{K_{O,H}+S_O}\right)X_{B,H}$
	Aerobic growth of heterotrophs from SMP	$\mu_{SMP}\left(\frac{S_{SMP}}{K_{SMP}+S_{SMP}}\right)\left(\frac{S_O}{K_{O,H}+S_O}\right)X_{B,H}$
2	Anoxic growth of heterotrophs	$\mu_H\left(\frac{S_S}{K_S+S_S}\right)\left(\frac{K_{O,H}}{K_{O,H}+S_O}\right)\left(\frac{S_{NO}}{K_{NO}+S_{NO}}\right)\eta_g X_{B,H}$
	Anoxic growth of heterotrophs from SMP	$\mu_{SMP}\left(\frac{S_{SMP}}{K_{SMP}+S_{SMP}}\right)\left(\frac{K_{O,H}}{K_{O,H}+S_O}\right)\left(\frac{S_{NO}}{K_{NO}+S_{NO}}\right)\eta_g X_{B,H}$
3	Aerobic growth of autotrophs	$\mu_A\left(\frac{S_{NH}}{K_{NH}+S_{NH}}\right)\left(\frac{S_O}{K_{O,A}+S_O}\right)X_{B,A}$
4	Decay of heterotrophs	$b_H X_{B,H}$
5	BAP formation from decay of heterotrophs	$b_{BAP,H} X_{B,H}$
6	Decay of autotrophs	$b_A X_{B,A}$
7	BAP formation from decay of autotrophs	$b_{BAP,A} X_{B,A}$
8	Ammonification of soluble organic nitrogen	$k_a S_{ND} X_{B,H}$
9	Hydrolysis of entrapped organics	$k_h \frac{X_S/X_{B,H}}{K_X+(X_S/X_{B,H})}\left[\left(\frac{S_O}{K_{O,H}+S_O}\right)+\eta_h\left(\frac{K_{O,H}}{K_{O,H}+S_O}\right)\left(\frac{S_{NO}}{K_{NO}+S_{NO}}\right)\right]X_{B,H}$
10	Hydrolysis of entrapped organic nitrogen	$\rho_9\left(X_{ND}/X_S\right)$

The reaction rate equation for component i can be computed from the sum:

$$r_i = \sum_j \nu_{ij}\rho_j \quad \text{overall processes } j$$

EMPIRICAL HYDRODYNAMIC MODEL

Activated sludge cross-flow velocity, U_{sr}:

$$U_{sr} = 1.311 U_{Lr}^{1.226} e^{-0.0105X}$$

Membrane fouling rate, K (defined as change in resistance over time, dR/dt):

$$K = 8.933 \times 10^{7} U_{Lr}^{-3.047} J^{0.376} X^{0.532}$$

Parameters:
U_{Lr} = tap water cross flow velocity (captures aeration intensity and reactor configuration)
X = suspended solids concentration
J = permeate flux

FRACTAL PERMEATION MODEL

Fractal model (used to determine pore area fractal dimension, D_s):

$$B(\geq a) = S_c - A = C_0 (a)^{2-D_s}$$

Cake permeability, K:

$$K = \frac{G}{g^2} C_0 \frac{1}{A_t} \frac{2-D_s}{3-D_s} a_{\max}^{3-D_s}$$

Parameters:
a = threshold pore area
S_c = total cake layer area
A = sum of all pore areas equal to or larger than a (i.e., $A = \sum a$)
C_0 = constant
D_s = pore area fractal dimension
G = geometry factor for fluid flow through a pore (i.e., $\pi/128$ for circular pores)
g = shape factor (i.e., $g = a/\lambda^2$ where a is the pore area and λ is the pore diameter)
A_t = total cake layer area
$a_{\max}$ = maximum pore area

SECTIONAL RESISTANCE MODEL

Total resistance: $R = R_m + R_p + R_{sf} + R_{sc}$

Membrane resistance: R_m

Pore fouling resistance: $R_p = r_p \sum J\theta_f$

Dynamic sludge film resistance: $R_{sf} = r_{sf} M_{sf}$

Stable sludge cake resistance: $R_{sc} = r_{sc} M_{sc}$

Mass of dynamic sludge film:

During filtration: $$\frac{dM_{sf}}{dt} = \frac{24CJ^2}{24J + C_d d_p G} - \frac{\beta(1-\alpha)GM_{sf}^2}{\gamma V_f t + M_{sf}}$$

During cleaning: $$\frac{dM_{sf}}{dt} = -\frac{\beta(1-\alpha)GM_{sf}^2}{0.1\gamma V_f \theta_f + M_{sf}}$$

Mass of stable sludge cake: ΔM_{sc} = remaining sludge after cleaning, which adds to the stable sludge cake layer

Assumed shear intensity profile:

$$\frac{G}{G_0} = \begin{cases} \frac{1}{10} + \frac{9}{20}\left[1 + \sin\frac{(2\varepsilon_i - \varepsilon_a)\pi}{2\varepsilon_a}\right] & \varepsilon_i < \varepsilon_a \\ 1 & \varepsilon_i \geq \varepsilon_a \end{cases}$$

Parameters:

r_p = specific pore fouling resistance

J = permeate flux

θ_f = filtration period of an operation cycle

r_{sf} = specific sludge film resistance

M_{sf} = mass of dynamic sludge film

r_{sc} = specific resistance of the sludge cake layer

M_{sc} = mass of stable sludge cake on membrane surface

C = sludge concentration

C_d = coefficient of the lifting force of a sludge particle

d_p = particle diameter

κ_r = maximum rate constant

κ_s = half-saturation constant

β = erosion rate coefficient of the dynamic sludge

α = stickiness of biomass particles

γ = compression coefficient for dynamic sludge
V_f = water production within the filtration period of operation cycle
t = filtration time
G_0 = apparent shear intensity of the fluid turbulence,
ε_i = accumulated membrane area fractions up to the ith section
ε_a = sectional area of membrane surface with reduced shear intensity (where G/G_0 is less than 1)

LEE ET AL. RESISTANCE-IN-SERIES MODEL

Total resistance: $R = R_m + \alpha k_m \dfrac{V_p X_{TSS}}{A}$

Parameters:
R_m = membrane resistance
α = specific resistance
k_m = cross-flow coefficient ranging from 0 to 1 (e.g. $k_m = 1$ for dead-end filtration)
V_p = permeate volume
X_{TSS} = concentration of total suspended solids (TSS) in the biomass
A = membrane surface area.

WINTGENS ET AL. RESISTANCE-IN-SERIES MODEL

Flux: $F = \dfrac{\Delta p_{TM}}{\eta_P \left(R_M + R_C + R_F \right)}$

Transmembrane pressure: $\Delta p_{TM} = p_{hydro} + p_{pump} - \Delta p_{ax}$

Cake resistance: $R_C = k_C c_b e^{F(t)/k_P}$ where $k_P = \dfrac{\tau_W d_C}{\eta_F}$

Fouling resistance: $R_F = S_F \left(1 - e^{-k_F \int_0^t F(t)dt} \right)$

$$\Longrightarrow \quad F(t) = \frac{p_{hydro} + p_{pump} + \Delta p_{ax}}{\eta_P \left(R_M + k_C c_b e^{F(t)/k_P} + S_F \left(1 - e^{-k_F \int_0^t F(t)dt} \right) \right)}$$

Parameters:

$F(t)$ = trans-membrane flux

η_P = permeate viscosity

p_{hydro} = hydrostatic pressure

p_{pump} = the suction pressure

Δp_{ax} = pressure loss from permeate flow along the hollow fibers

R_m = membrane resistance

k_C = cake layer model parameter

c_b = bulk concentration

k_P = local mass transfer coefficient

τ_W = mean wall shear stress

d_C = characteristic particle diameter

η_F = viscosity of the activated sludge

S_F = model parameter for fouling saturation

k_F = model parameter for fouling

$\int_0^t F(t)dt$ = total permeate volume per membrane area produced between two chemical cleanings

REFERENCES

Barker, D. J. and D. C. Stuckey (1999). "A review of soluble microbial products (SMP) in wastewater treatment systems." Water Research **33**(14): 3063-3082.

Bird, R. B., W. E. Stewart and E. N. Lightford (1960). Transport Phenomena. New York, Wiley.

Breu, A. P. J., H. M. Ensner, C. A. Kruelle and I. Rehberg (2003). "Reversing the Brazil-nut effect: Competition between percolation and condensation." Physical Review Letters **90**(1): 014302.

Brinkman, H. C. (1947). "A calculation of the viscous force exerted by a flowing fluid on a dense swarm of particles." Appl. Sci. Res. **A1**: 27-34.

Brinkman, H. C. (1947). "On the permeability of media crossing of closely packed porous particles." Appl. Sci. Res. **A1**: 81.

Carman, P. C. (1937). "Fluid flow through a granular bed." Transactions of Institute of Chemical Engineers **15**: 150-156.

Chellam, S. (2005). "Artificial neural network model for transient crossflow microfiltration of polydispersed suspensions." Journal of Membrane Science **258**(1-2): 35-42.

Chellman, S. and M. R. Wiesner (1998). "Evaluation of crossflow filtration models based on shear-induced diffusion and particle adhesion: Complications induced by feed suspension polydispersity." Journal of Membrane Sicence **138**: 83-97.

Davis, R. H. and S. A. Birdsell (1987). "Hydrodynamic model and experiments for crossflow microfiltration." Chemical Engineering Communication **49**: 217-234.

Davis, R. H. and D. T. Leighton (1987). "Shear-induced transport of a particle layer along a porous wall." Chemical Engineering Science **42**(2): 275-281.

Davis, R. H. and J. D. Sherwood (1990). "A similarity solution for steady-state crossflow microfiltration." Chemical Engineering Science **45**(11): 3203-3209.

de Silva, D. G. V., V. Urbain, D. H. Abeysinghe and B. E. Rittmann (1998). "Advanced analysis of membrane-bioreactor performance with aerobic-anoxic cycling." Water Science and Technology **38**(4-5): 505-512.

Furumai, H. and B. E. Rittmann (1992). "Advanced modeling of mixed populations of heterotrophs and nitrifiers considering the formation and exchange of soluble microbial products." Water Science and Technology **26**(3-4): 493-502.

Geissler, S., T. Wintgens, T. Melin, K. Vossenkaul and C. Kullmann (2005). "Modelling approaches for filtration processes with novel submerged capillary modules in membrane bioreactors for wastewater treatment." Desalination **178**(1-3): 125-134.

Gmachowski, L. (1998). "Flow drag in polydisperse systems." Water Research **32**(9): 2655-2659.

Gujer, W., M. Henze, T. Mino and M. van Loosdrecht (1999). "Activated sludge model No. 3." Water Science and Technology **39**(1): 183-193.

Happel, J. (1958). "Viscous flow in multiparticle systems: slow motion of fluids relative to beds of spherical particles." AIChE Journal **4**: 197-201.

Happel, J. and H. Brenner (1965). Low Reynolds Number Hydrodynamics. Englewood Cliffs, NJ, Prentice-Hall, Inc.

Henze, M., C. P. L. J. Grady, W. Gujer, G. v. R. Marais and T. Matsuo (1987). Activated Sludge Model No. 1. IAWPRC Scientific and Technical Report No. 1. London, IAWPRC.

Henze, M., W. Gujer, T. Mino, T. Matsuo, M. C. Wentzel and G. v. R. Marais (1995). Activated Sludge Model No. 2. IAWQ Scientific and Technical Report No. 3. London, IAWQ.

Henze, M., W. Gujer, T. Mino, T. Matsuo, M. C. Wentzel, G. v. R. Marais and M. C. M. Van Loosdrecht (1999). "Activated sludge model No.2d, ASM2d." Water Science and Technology **39**(1): 165-182.

Henze, M., W. Gujer, T. Mino and M. van Loosdrecht (2000). Activated Sludge Models: ASM1, ASM2, ASM2d, and ASM3. London, IWA Publishing.

Hinch, E. J. (1977). "An averaged-equation approach to particle interactions in a fluid suspension." Journal of Fluid Mechanics **83**: 695--720.

Howells, I. D. (1974). "Drag due to the motion of a Newtonian fluid through a sparse random array of small fixed rigid objects." Journal of Fluid Mechanics **64**: 449--475.

Huang, X., R. Liu and Y. Qian (2000). "Behaviour of soluble microbial products in a membrane bioreactor." Process Biochemistry **36**(5): 401-406.

Kaye, B. H. (1994). A Random Walk Through Fractal Dimensions. New York, VCH: Chapter 6.

Kim, S. and W. B. Russel (1985). "Modeling of porous media by renormalization of the Stokes equations." Journal of Fluid Mechanics **154**: 269--286.

Knight, J. B., H. M. Jaeger and S. R. Nagel (1993). "Vibration-induced size separation in granular media: The convection connection." Physical Review Letters **70**: 3728-3731.

Lamb, H. (1932). Hydrodynamics. New York, Dover Publications.

Lee, Y., J. Cho, Y. Seo, J. W. Lee and K.-H. Ahn (2002). "Modeling of submerged membrane bioreactor process for wastewater treatment." Desalination **146**(1-3): 451-457.

Leighton, D. and A. Acrivos (1987). "Measurement of the shear induced coefficient of self-diffusion in concentration suspensions of spheres." Journal of Fluid Mechanics **177**: 109-131.

Li, X.-Y. and X.-M. Wang "Modelling of membrane fouling in a submerged membrane bioreactor." Journal of Membrane Science **In Press, Corrected Proof.**

Liu, R., X. Huang, Y. F. Sun and Y. Qian (2003). "Hydrodynamic effect on sludge accumulation over membrane surfaces in a submerged membrane bioreactor." Process Biochemistry **39**(2): 157-163.

Lu, S.-Y. and C.-M. Tsai (2000). "Membrane microstructure resulting from deposition of polydisperse particles." Journal of Membrane Science **177**(1-2): 55-71.

Lu, S. G., T. Imai, M. Ukita, M. Sekine, T. Higuchi and M. Fukagawa (2001). "A model for membrane bioreactor process based on the concept of formation and degradation of soluble microbial products." Water Research **35**(8): 2038-2048.

Mallevialle, J., P. E. Odendaal and M. R. Wiesner (1996). The Emergence of Membranes in Water and Wastewater Treatment. Water Treatment Membrane Processes. J. Mallevialle, P. E. Odendaal and M. R. Wiesner. New York, McGraw-Hill: 17.1-17.31.

Manem, J. and R. Sanderson (1996). Membrane Bioreactors. Water Treatment Membrane Processes. J. Mallevialle, P. E. Odendaal and M. R. Wiesner. New York, McGraw-Hill: 17.1-17.31.

Mendenhall, W., R. J. Beaver and B. M. Beaver (2003). Introduction to Probability and Statistics. Pacific Grove, CA, Brooks/Cole.

Meng, F., H. Zhang, Y. Li, X. Zhang and F. Yang (2005). "Application of fractal permeation model to investigate membrane fouling in membrane bioreactor." Journal of Membrane Science **262**(1-2): 107-116.

Mondor, M. and C. Moresoli (2000). "Experimental verification of the shear-induced hydrodynamic diffusion model of crossflow microfiltration, with consideration of the transmembrane pressure axial variation." Journal of Membrane Science **175**(1): 119-137.

Park, N., B. Kwon, I. S. Kim and J. Cho (2005). "Biofouling potential of various NF membranes with respect to bacteria and their soluble microbial products (SMP): Characterizations, flux decline, and transport parameters." Journal of Membrane Science **258**(1-2): 43-54.

Romero, C. A. and R. H. Davis (1988). "Global model of crossflow microfiltration based on hydrodynamic particle diffusion." Journal of Membrane Science **39**: 157-185.

Rosenberger, S., C. Laabs, B. Lesjean, R. Gnirss, G. Amy, M. Jekel and J. C. Schrotter (2006). "Impact of colloidal and soluble organic material on membrane performance in membrane bioreactors for municipal wastewater treatment." Water Research **40**(4): 710-720.

Russel, W. B., D. A. Saville and W. R. Schowalter (1989). Colloidal Dispersions. New York, Cambridge Univ. Press.

Sethi, S. and M. R. Wiesner (1997). "Modeling of transient permeate flux in cross-flow membrane filtration incorporating multiple particle transport mechanisms." Journal of Membrane Science **136**: 191-205.

Shin, H.-S. and S.-T. Kang (2003). "Characteristics and fates of soluble microbial products in ceramic membrane bioreactor at various sludge retention times." Water Research **37**(1): 121-127.

Soppe, W. (1990). "Computer simulation of random packings of hard spheres." Powder Technology **62**: 189-196.

Tchobanoglous, G., F. L. Burton and H. D. Stensel (2004). Wastewater Engineering: Treatment and Reuse. Boston, McGraw-Hill: 854-865.

Urbain, V., B. Mobarry, V. de Silva, D. A. Stahl, B. E. Rittmann and J. Manem (1998). "Integration of performance, molecular biology and modeling to describe the activated sludge process." Water Science and Technology **37**(4-5): 223-229.

Wintgens, T., J. Rosen, T. Melin, C. Brepols, K. Drensla and N. Engelhardt (2003). "Modelling of a membrane bioreactor system for municipal wastewater treatment." Journal of Membrane Science **216**(1-2): 55-65.

Xu, X. Y., J. R. Xu and Y. Kang (1995). "Dynamics of air pressure filtration and fractal filter cake constructure." Journal of Chemical Industrial Engineering **46**: 8-14.

Yang, W., N. Cicek and J. Ilg (2006). "State-of-the-art of membrane bioreactors: Worldwide research and commercial applications in North America." Journal of Membrane Science **270**(1-2): 201-211.